

# Asymptotic Formulation of the Role of Shear Loads on Multi-Layered Thin Shells and Classification of Their Deformation Modes

Xiwei Pan<sup>a</sup>, Yichao Zhu<sup>a,b,\*</sup>

<sup>a</sup>Department of Engineering Mechanics, Dalian University of Technology, Dalian, 116023, P. R. China

<sup>b</sup>State Key Laboratory of Structural Analysis, Optimization and CAE Software for Industrial Equipment, Dalian University of Technology

---

## Abstract

Shell structures are generally modeled based on kinematic hypotheses, where some of the parameters are preferentially evaluated in a phenomenological manner. In this article, asymptotic analysis against the underlying three-dimensional equation system is considered so as to provide a rational framework for modeling and interpreting the deformation behavior of multi-layered thin shells (MTSs). Capable of accurate predictions of not only the overall stiffness of MTSs, but also the detailed stress distribution, the proposed shell theory shows its distinguishing features at least in the following aspects. Firstly, it naturally introduces a rule for classifying the deformation modes of MTSs. One mode resembles a plate, where the transverse load is withstood through bending, while the other is like a supporting structure, where the load gets conducted to adjacent inclined sections. Secondly, in contrast with the existing arguments where an applied shear load on the shell surface necessitates the inclusion of transverse shear stresses for analysis, it is demonstrated that a leading-order multi-layered shell theory derived from asymptotic analysis should suffice to output satisfactory predictions over the shell stiffness, as well as its internal stress distribution. Numerical examples of the deformation and strength analysis for MTSs are also presented to show the reliability of the leading-order model.

*Keywords:* Multi-layered thin shell, Surface shear force, Transverse shear stress, Shell strength, Asymptotic analysis, Isogeometric analysis

---

## 1. Introduction

Shell structures, owing to their excellence in load-bearing behavior and containment of space, have seen extensive applications across various engineering disciplines including civil, aerospace, biomechanics, etc. Moreover, they offer a visually striking and aesthetically pleasing solution for the realm of architectural design.

Multi-layered thin shells (MTSs), as a crucial component thereof, further enhance the versatility of material distribution to accommodate various external loading conditions and deformation patterns. Due to the geometric characteristics of such structures, where the dimension along shell thickness direction is significantly smaller than the other two surface dimensions, conducting three-dimensional (3D) solid-based analyses using direct brick elements or solid shell elements (Klinkel et al. (1999)) entails substantial computational overhead in order to accurately capture the stress variation along that direction, which is a cumbersome yet unnecessary task. A prevalent approach involves introducing assumptions regarding structural responses implied by the geometry, thereby associating internal field variables with the mid-surface of the shell to derive a degenerated two-dimensional (2D) model. This facilitates problem analysis while allowing the outcomes to be readily extrapolated to the entire configuration based on the presumed response patterns.

In the majority of prior endeavors to address aforementioned 3D-to-2D transformation, pioneered by Love (1892), Reissner (1941), Reissner (1952), Naghdi (1957a), Naghdi (1957b), Sanders (1960), Koiter (1960), considerable attention has been devoted to establishing appropriate stress-strain relations that are compatible with the original 3D constitutive equations of the structure. In general, there are two

---

\*Corresponding authors

Email address: yichaozhu@dlut.edu.cn (Yichao Zhu)

primary implementations: the axiomatic approach and the asymptotic approach. The former requires a “*priori* guess” regarding the deformation modes of the shell under consideration, often informed by experimental or empirical insights. According to this assumption, shell deformation can be approximately described by the stretching and bending of its mid-surface. From the earliest days of Love’s introduction of Kirchhoff’s assumptions on plate bending to the solution for isotropic shells (Love (1892)), axiom-based shell theories have come a long way, but they have basically revolved around the quest for more accurate modeling of transverse stresses. In classical shell theory (CST), the well-known Kirchhoff-Love hypothesis postulates a state of plane strain while simultaneously neglecting the effect of transverse stresses in the stress-strain relationships. This yields a set of governing equations for three displacements on the shell mid-surface, effectively characterizing the mechanical response of isotropic homogeneous thin shells, and the corresponding error introduced by the simplification is roughly of  $\mathcal{O}(h/R)$  (Koiter (1960)), where  $h$  is the overall thickness and  $R$  denotes the minimum principal radius of curvature of the shell mid-surface. However, due to trivial transverse strains, CST is limited in its applicability to more complex scenarios, such as shear deformation.

In response to the problems mentioned above, the subsequent improved theories partially or completely discard the Kirchhoff-Love hypothesis including assumptions regarding the smallness of  $h/R$  and the non-deformability of the normal. Byrne (1944), Flügge (2013) and Vlasov (1951) were more careful in their treatment of  $h/R$ , retaining terms that were initially considered negligible in the strain-displacement relationships as well as in the stress resultant equations. These terms were then expanded into a series, with only the first few terms retained for approximation. In contrast to the results obtained directly from the Kirchhoff-Love hypothesis, which are called “the first-order approximations”, theories derived along this line are referred to as “the second-order approximations”. Another class of second-order approximations enjoy a solid foundation rooted in the variational principle proposed by Reissner (1950) and take into account the effects of transverse shear and normal stresses by either choosing more flexible expressions for displacement along the surface normal (Naghdi (1957a)), directly incorporating effects of thickness variation into the transverse stress components (Naghdi (1957b)), or a combination of both (Reissner (1952)). Similar to the aforementioned methods, none of these approaches provide solid, explicit reasons for these choices or a discussion on the need for modifications.

Reissner-Mindlin theory, also known as the first-order shear deformation theory (FSDT), was first proposed by Reissner (1945) and Mindlin (1951) for elastic plates and then extended to laminated shells (Dong & Tso (1972)). This hypothesis partially discards the assumption of an undeformable normal while retaining the original inextensible constraint. The theory introduces two new variables in the in-plane displacements to account for normal rotations and incorporates constitutive equations for transverse shear stresses. The shear correction factor (SCF)  $K$  is adopted to partially address inaccuracies arising from the uniform distribution of shear strains along the thickness direction, thereby providing accurate strain energy contributions. For isotropic homogeneous elastic problems, as suggested by Reissner (1945), a commonly used value for  $K$  is  $\frac{5}{6}$ , while specific values catering for more complicated cases such as orthotropic laminates (Whitney (1973)), sandwich structures (Birman & Bert (2002)) and layered plates and shells (Gruttmann & Wagner (2017)) are also available, albeit requiring much more effort. The diversity in the value of  $K$  reflects, to some extent, the ongoing need for improvement in the FSDT.

For multi-layered or laminated shells, analyses based on the FSDT encounter challenges. Firstly, the uniformly distributed transverse shear strain fails to accurately capture the true distribution in multi-layered structures. Secondly, determining the SCF for shells with complex cross-sections poses difficulties. In this context, higher order theories (HOTs) turn out to be more appropriate for considering shear effects, where more enriched kinematic assumptions for the displacement field are generally adopted. When the assumed displacement patterns are applied to all layers simultaneously, it leads to the equivalent single layer (ESL) method (Abrate & Di Sciuva (2017), Tornabene et al. (2022a)), which is computationally efficient as the unknowns are independent of the number of material layers. However, it struggles to satisfy interlaminar stress continuities and surface boundary conditions. In contrast, layerwise theories (LWTs) apply the assumed patterns independently to each ply (Barbero et al. (1990), Tornabene et al. (2022b)), ensuring perfect bonding between plies. However, LWTs require a large number of degrees of freedom to model each stack layer individually. The advantages of the above two can be integrated within the framework of zigzag theories (refer to the review work of Carrera (2003a) for more details). These models tend to address shear deformation by employing more complex expressions, such as higher-order or piecewise functions, a path that seems endless. Furthermore, they rarely evaluate how shear deformation

affects the internal stress distribution of such structures to assess whether this level of complexity is necessary.

The aforementioned axiomatic approaches pursue a more accurate modeling of shells by either pre-assuming the displacement expressions or adding terms without clear physical backgrounds. These operations introduce many ambiguities to the analytical process. For instance, while dropping, retaining and adding certain terms in various literatures do improve the accuracy of the original theory to some extent, the exact order of their effects is difficult to assess. And most likely, as Koiter (1960) pointed out, many apparently different refinements of the first approximation are essentially of the same order of magnitude. To address such an issue, asymptotic approaches (Cicala (1965), Ciarlet & Lods (1996), Carrera (2001), Carrera (2003b), Ciarlet & Mardare (2019), Zhao et al. (2022), Zhao & Zhu (2023)) have been proposed to provide approximate shell formulations with known accuracy from a mathematically rigorous perspective. Theories of this type typically feature a small parameter implied by physical characteristics, with the corresponding variables and equations expressed as series expansions. This allows the shell equations to be truncated to the desired order. Chien (1944) introduced two tensors defined on the mid-surface and derived the complete intrinsic theories of elastic plates and shells from the 3D theory based on Taylor expansions. Carrera (2003b) and Carrera et al. (2014) later proposed a unified method, i.e., the Carrera unified formulation (CUF), by choosing a more general expansion form for the displacement field. And the axiomatic/asymptotic technique has been subsequently developed under the CUF framework, which presents systematic asymptotic analyses based on initially-assumed expressions. The error caused by the deactivation of each term included in the expressions is studied thoroughly, resulting in a suitable displacement pattern consisting of all significant terms. Note also that, the classical plate theory based on the Kirchhoff-Love hypothesis can be justified by the asymptotic method (Zhao et al. (2022)). Despite having encompassed all terms whose influences are of the same order of magnitude, the development of asymptotic approaches turns out to be more difficult than axiom-based approaches, mainly due to the need to address separate analysis for each parameter. So, for such methods, it is crucial to achieve satisfactory accuracy at the first few orders or even at the leading order. In plate structures, especially microstructural plates (Zhao & Zhu (2023)), a leading-order asymptotic theory has been shown to be sufficient for modeling the main behavior without the need to account for additional transverse shear strain effects.

In this paper, we propose a method based on AA for a more rational modeling of MTSs and interpretation of shell deformation modes. Through AA, we identify two shell deformation patterns, and the specific orders of relevant quantities such as the displacement and stress components, external loads, observation time, are also determined for both weakly and normally curved shells. Most importantly, the applied shear forces are revealed to affect the redistribution of local in-plane stress components. Therefore, contrary to existing arguments where an applied shear force requires the inclusion of transverse shear stresses for modeling, this approach demonstrates that a leading-order asymptotic shell theory is sufficient to capture the shell stiffness and the desired stress distribution with satisfactory accuracy. To be specific, we first examine the asymptotic behavior of the full 3D equations of MTSs based on their intrinsic thinness. Regarding the non-dimensionalization of certain field variables, i.e., displacement and stress fields, we directly follow the conclusions drawn from plate problems (Reissner (1941), Zhao et al. (2022)) and apply them locally to shell structures. However, due to the varying geometries of real-world shell configurations, the order of the dimensionless principal curvatures  $\hat{\kappa}_\alpha$  cannot be uniquely determined, e.g., they equal 1 for a spherical shell, whereas for a nearly flat shell, they approach 0 and become negligible. Consequently, the derivation begins to bifurcate depending on the specific magnitude of the maximum (dimensionless) principal curvature. The case-by-case analysis facilitates a comprehensive understanding of both the common features and the distinct deformation modes present in each scenario. Moreover, by leveraging the commonalities between the two cases, we can readily derive a unified formulation of MTSs. Corresponding numerical examples are implemented through isogeometric discretization (Hughes et al. (2005)).

The remainder of this article is organized as follows: Sec. 2 presents basic settings regarding the problem including the representation of shell geometry, three basic equations formulated in the orthogonal curvilinear coordinate system and the investigated boundary conditions. With the introduction of a small parameter implied by geometric thinness, AA is performed on these equations. Cases of weakly and normally curved shells and the unified shell formulations are elaborated in Sec. 3. In Sec. 4, we generally start from the principle of virtual work to derive the variational formulation of MTSs, and the

isogeometric discretization is then adopted for numerical implementation. This is followed by several validations shown in Sec. 5, the proposed multi-layered shell model should first pass three shell obstacle problems to be deemed as qualified, and then, the free vibration problems, as well as examples where surface shear forces exist are considered for spherical, cylindrical and ellipsoidal shells. All the examined examples are compared with the results obtained from finite element analysis (FEA) with extremely fine mesh so as to demonstrate the model reliability and to elucidate the true role of surface shear forces. Finally, Sec. 6 concludes the article.

## 2. Problem Settings

### 2.1. Shell Geometry

An MTS consisting of  $N$  layers, where the thickness ratio of each layer from bottom to top with respect to the overall thickness  $h$  is denoted by  $\lambda_{\mathcal{L}}$ ,  $\mathcal{L} = 1 \cdots, N$ , is considered here first, with a detailed illustration shown in Fig. 1. For the referenced geometry of the shell mid-surface, it can be generally parametrized by

$$\mathcal{S} : \mathbf{r} = \mathbf{r}(\widehat{\xi}_1, \widehat{\xi}_2), \quad (1)$$

where  $\widehat{\xi}_\alpha$ ,  $\alpha = 1, 2$  are two selected parameters, and the symbol “ $\wedge$ ” attached to a variable represents its non-dimensional counterpart. Thus the length scale is actually stored in  $\mathbf{r}$ . To facilitate further analysis, unless specified, Greek letters are adopted throughout the article to indicate components associated with the tangent plane at each point, e.g.,  $\alpha = 1, 2$ , and Latin letters are used to represent quantities that take values in the whole three-dimensional space, e.g.,  $i = 1, 2, 3$ .

Based on the mid-surface representation given by Eq. (1), any point inside an MTS of thickness  $h$  can be obtained by offsetting a specific point on  $\mathcal{S}$  by  $h \widehat{\xi}_3 \mathbf{e}_3$  along the normal direction  $\mathbf{e}_3$ , that is,

$$\Omega : \mathbf{r}_s = \mathbf{r}(\widehat{\xi}_1, \widehat{\xi}_2) + h \widehat{\xi}_3 \mathbf{e}_3, \quad (2)$$

where  $\mathbf{e}_3$ , as illustrated in Fig. 1, is the unit normal to the shell mid-surface  $\mathcal{S}$ , and  $\widehat{\xi}_3$  takes its values within the range  $[-0.5, 0.5]$ .

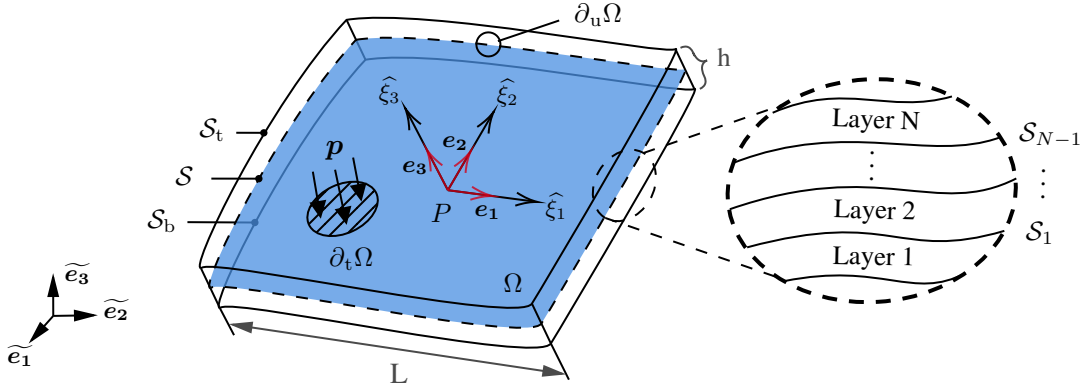


Figure 1: Representation of the multi-layered thin shell. The overall shell entity is denoted by  $\Omega$  and the shell mid-surface (blue part) is denoted by  $\mathcal{S}$ , with  $\mathcal{S}_b$  and  $\mathcal{S}_t$  being the bottom and top surfaces of the structure, respectively.  $\mathcal{S}_I$  ( $I = 1, \cdots, N - 1$ ) represents the interface between two adjacent layers  $I$  and  $(I + 1)$ . A set of orthogonal curvilinear coordinate systems  $(\widehat{\xi}_1, \widehat{\xi}_2, \widehat{\xi}_3)$  is attached to  $\mathcal{S}$ , and the corresponding in-plane orthonormal basis vectors  $\mathbf{e}_\alpha$  are aligned to the local principal directions of the shell mid-surface. Another orthonormal basis  $\{\widetilde{\mathbf{e}}_1, \widetilde{\mathbf{e}}_2, \widetilde{\mathbf{e}}_3\}$  are aligned to directions of the global Cartesian coordinate system.

Without loss of generalities, one can always choose coordinates  $\widehat{\xi}_\alpha$ ,  $\alpha = 1, 2$  that parameterize “lines of curvature” except at umbilical points of the regular surface, which then yields an orthogonal curvilinear coordinate system  $(\widehat{\xi}_1, \widehat{\xi}_2, \widehat{\xi}_3)$ . Accordingly, the first and second fundamental forms of the mid-surface with respect to two parameters are both diagonal, i.e.,

$$\frac{\partial \mathbf{r}}{\partial \widehat{\xi}_\alpha} \cdot \frac{\partial \mathbf{r}}{\partial \widehat{\xi}_\beta} = 0; \quad \frac{\partial^2 \mathbf{r}}{\partial \widehat{\xi}_\alpha \partial \widehat{\xi}_\beta} \cdot \mathbf{e}_3 = 0, \quad (3)$$

where the subindices satisfy  $\alpha \neq \beta$ . Therefore, an orthonormal basis  $\{\mathbf{e}_1, \mathbf{e}_2, \mathbf{e}_3\}$ , as shown in Fig. 1, is defined on the tangent plane of a given point  $P$  on the shell mid-surface by

$$\mathbf{e}_\alpha = \frac{1}{a_\alpha} \frac{\partial \mathbf{r}}{\partial \widehat{\xi}_\alpha}; \quad \mathbf{e}_3 = \mathbf{e}_1 \times \mathbf{e}_2, \quad (4)$$

note that the Einstein summation convention is not adopted here, nor will it be adopted later unless specified. And  $a_\alpha$  above take the expressions

$$a_\alpha \left( \widehat{\xi}_1, \widehat{\xi}_2 \right) = \left| \frac{\partial \mathbf{r}}{\partial \widehat{\xi}_\alpha} \right|. \quad (5)$$

Alternatively, the basis vectors  $\mathbf{e}_i$  can be defined, from the perspective of space  $\Omega$  which is occupied by the shell entity (Eq. (2)), by

$$\mathbf{e}_i = \frac{1}{h_i} \frac{\partial \mathbf{r}_s}{\partial \widehat{\xi}_i}; \quad h_i \left( \widehat{\xi}_1, \widehat{\xi}_2, \widehat{\xi}_3 \right) = \left| \frac{\partial \mathbf{r}_s \left( \widehat{\xi}_1, \widehat{\xi}_2, \widehat{\xi}_3 \right)}{\partial \widehat{\xi}_i} \right|, \quad (6)$$

where  $h_i \left( \widehat{\xi}_1, \widehat{\xi}_2, \widehat{\xi}_3 \right)$  are the *Lamé coefficients*.

Derivatives of the above basis vectors can be expressed based on the linear combination of themselves in general, that is,

$$\frac{\partial \mathbf{e}_i}{\partial \widehat{\xi}_j} = \sum_k \Gamma_{ijk} \mathbf{e}_k, \quad (7)$$

the related coefficients  $\Gamma_{ijk}$  are called the *Christoffel symbols*. Having determined the 27 constants  $\Gamma_{ijk}$ , the expressions of the specific derivatives become

$$\frac{\partial \mathbf{e}_i}{\partial \widehat{\xi}_j} = \frac{\mathbf{e}_j}{h_i} \frac{\partial h_j}{\partial \widehat{\xi}_i} - \delta_{ij} \sum_k \frac{\mathbf{e}_k}{h_k} \frac{\partial h_i}{\partial \widehat{\xi}_k}, \quad (8)$$

and one can refer to the works of [Reissner \(1941\)](#) and [Howell et al. \(2008\)](#) for detailed derivations.

To determine the mathematical expressions of the *Lamé coefficients*  $h_i$ , one has to first calculate the terms  $\partial \mathbf{e}_3 / \partial \widehat{\xi}_\alpha$ . Since the principal curvatures of a regular parametric surface  $\mathcal{S}$  at a point  $P$  are exactly associated with the two eigenvalues of the corresponding *Weingarten map* of that point, which is defined as a tangent map  $g_*$  from the tangent space  $T_P \mathcal{S}$  to itself:  $W = -g_* : T_P \mathcal{S} \rightarrow T_P \mathcal{S}$ , we have the following relation

$$W(\mathbf{e}_\alpha) = -\frac{1}{a_\alpha} g_* \left( \frac{\partial \mathbf{r}}{\partial \widehat{\xi}_\alpha} \right) = -\frac{1}{a_\alpha} \frac{\partial \mathbf{e}_3}{\partial \widehat{\xi}_\alpha} = \kappa_\alpha \mathbf{e}_\alpha, \quad (9)$$

where  $\kappa_\alpha \left( \widehat{\xi}_1, \widehat{\xi}_2 \right)$  are the principal curvatures of the shell mid-surface.

Based on Eqs. (4) and (9), the derivatives of shell parametrization  $\mathbf{r}_s$  taken with respect to the curvilinear coordinates are expressed by

$$\frac{\partial \mathbf{r}_s}{\partial \widehat{\xi}_\alpha} = a_\alpha \left( 1 - h \kappa_\alpha \widehat{\xi}_3 \right) \mathbf{e}_\alpha; \quad \frac{\partial \mathbf{r}_s}{\partial \widehat{\xi}_3} = h \mathbf{e}_3, \quad (10)$$

so the *Lamé coefficients*  $h_i$  take the form

$$h_\alpha = a_\alpha \left( 1 - h \kappa_\alpha \widehat{\xi}_3 \right); \quad h_3 = h. \quad (11)$$

## 2.2. Basic Equations in Orthogonal Curvilinear Coordinate Systems

Based on the global-to-local coordinate transformation in shell representation mentioned above, one can write down the three-dimensional governing equations for an MTS in the curvilinear coordinate system, i.e.,

(1) the dynamic equilibrium equations in the curvilinear coordinates read

$$\rho \ddot{u}_i = \mathbf{e}_i \cdot (\nabla \cdot \boldsymbol{\sigma}) + f_i = \sum_j \frac{1}{H} \frac{\partial}{\partial \widehat{\xi}_j} \left( \frac{H \sigma_{ij}}{h_j} \right) + \sum_k \frac{1}{h_i h_k} \left( \sigma_{ik} \frac{\partial h_i}{\partial \widehat{\xi}_k} - \sigma_{kk} \frac{\partial h_k}{\partial \widehat{\xi}_i} \right) + f_i, \quad (12)$$

where  $\ddot{u}_i = \frac{\partial^2 u_i}{\partial t^2}$  and  $H = h_1 h_2 h_3$ ;

(2) the strain components read

$$\varepsilon_{ij} = \frac{1}{2} \left( \frac{1}{h_j} \frac{\partial u_i}{\partial \widehat{\xi}_j} - \frac{u_i}{h_i h_j} \frac{\partial h_i}{\partial \widehat{\xi}_j} + \frac{1}{h_i} \frac{\partial u_j}{\partial \widehat{\xi}_i} - \frac{u_j}{h_i h_j} \frac{\partial h_j}{\partial \widehat{\xi}_i} \right) + \delta_{ij} \sum_k \frac{u_k}{h_j h_k} \frac{\partial h_j}{\partial \widehat{\xi}_k}; \quad (13)$$

one also needs the (3D) constitutive laws to close the system. At each point in  $\Omega$ , the local curvilinear coordinate basis is found by rotating the usual Cartesian basis  $\{\tilde{\mathbf{e}}_1, \tilde{\mathbf{e}}_2, \tilde{\mathbf{e}}_3\}$ , and the rotation is characterized by an orthogonal matrix  $\mathbf{Q}$  whose rows are the basis vectors as defined by Eq. (4), that is,  $\mathbf{Q} = (\mathbf{e}_1, \mathbf{e}_2, \mathbf{e}_3)^T$ . Thus a congruent transformation linking two second-order tensors in different orthogonal coordinates, such as  $\mathbf{A} = (a_{ij})$  in  $\{\mathbf{e}_1, \mathbf{e}_2, \mathbf{e}_3\}$  and  $\mathbf{B} = (b_{ij})$  in  $\{\tilde{\mathbf{e}}_1, \tilde{\mathbf{e}}_2, \tilde{\mathbf{e}}_3\}$ , can be expressed based on the above orthogonal matrix  $\mathbf{Q}$

$$\mathbf{A} = \mathbf{Q} \mathbf{B} \mathbf{Q}^T \quad \text{or} \quad a_{ij} = \mathbf{e}_i^T \mathbf{B} \mathbf{e}_j. \quad (14)$$

When considered in a fixed Cartesian coordinate system, the constitutive laws read

$$\sigma_{ij} = \lambda (\varepsilon_{kk}) \delta_{ij} + 2G \varepsilon_{ij}, \quad (15)$$

where the two coefficients  $\lambda$  and  $G$  are called the “*Lamé constants*”. Based on the orthonormal basis vectors in such a coordinate system, Eq. (15) can be re-expressed in the form of tensor

$$\sigma_{ij} \tilde{\mathbf{e}}_i \tilde{\mathbf{e}}_j^T = \lambda (\varepsilon_{kk}) \delta_{ij} \tilde{\mathbf{e}}_i \tilde{\mathbf{e}}_j^T + 2G \varepsilon_{ij} \tilde{\mathbf{e}}_i \tilde{\mathbf{e}}_j^T, \quad (16)$$

it is noted that, the Einstein summation rule is adopted in the above two equations. And the congruent transformation (Eq. (14)) indicates that the constitutive laws remain unchanged in different orthogonal coordinate systems.

### 2.3. Boundary Conditions

For the investigated MTS, the following boundary conditions are involved for both surfaces (top and bottom) and interfaces (between laminate layers). Firstly, on the shell surfaces, we have

$$\sigma_{\alpha 3} = p_\alpha \left( \widehat{\xi}_1, \widehat{\xi}_2 \right), \quad \widehat{\xi}_3 = \frac{1}{2}; \quad \sigma_{33} = p_3 \left( \widehat{\xi}_1, \widehat{\xi}_2 \right), \quad \widehat{\xi}_3 = \frac{1}{2}; \quad \sigma_{i3} = 0, \quad \widehat{\xi}_3 = -\frac{1}{2}, \quad (17)$$

where  $p_i$  are the external loads per area imposed on the top surface of the shell  $\mathcal{S}_t$ .

Secondly, on the interface of any two adjacent layers, all the displacement components measured in the local curvilinear coordinate system should remain continuous. Thus

$$u_i|_{\widehat{\xi}_3}^{\pm} = 0, \quad \text{on } \widehat{\xi}_3 = \mathcal{S}_I, \quad (18)$$

where  $u_i|_{\widehat{\xi}_3}^{\pm}$  represents the difference in the values of  $u_i$  on both sides of the interface, and  $\mathcal{S}_I$  denotes the  $\widehat{\xi}_3$ -coordinate of the interface between the  $I$ -th and  $(I+1)$ -th layer,  $I = 1, 2, \dots, N-1$ . Moreover, the transverse stress components between layers should also be continuous, that is,

$$\sigma_{i3}|_{\widehat{\xi}_3}^{\pm} = 0, \quad \text{on } \widehat{\xi}_3 = \mathcal{S}_I. \quad (19)$$

### 3. Asymptotic Reduction of the 3D Governing Systems for the MTS

#### 3.1. Non-dimensionalization

In view of the slender nature of an MTS, and a small parameter  $\epsilon$  is thus introduced by

$$\epsilon = \frac{h}{L} \ll 1, \quad (20)$$

where  $L$  is a parameter characterizing the shell surface dimension, while  $h$  is recalled to be the shell thickness.

For AA, the 3D equations listed above are preferably non-dimensionalized, and generally, non-dimensionalization is carried out in three aspects: (1) surface geometry; (2) material properties (3) field variables. Firstly, for quantities that characterize the surface geometry, the typical length scale  $L$  is selected as the reference, that is,

$$\mathbf{r}(\widehat{\xi}_1, \widehat{\xi}_2) = L \widehat{\mathbf{r}}(\widehat{\xi}_1, \widehat{\xi}_2); \quad a_\alpha(\widehat{\xi}_1, \widehat{\xi}_2) = L \widehat{a}_\alpha(\widehat{\xi}_1, \widehat{\xi}_2); \quad \kappa_\alpha = \frac{1}{L} \widehat{\kappa}_\alpha, \quad (21)$$

here the symbol “ $\widehat{\phantom{x}}$ ” is recalled to denote a non-dimensional quantity. One thing worth mentioning is that the dimensionless principal curvatures  $\widehat{\kappa}_\alpha$  here cannot be hastily assumed to be of  $\mathcal{O}(1)$ , as diverse geometries of shell structures encompasses cases where principal curvatures approach zero, e.g., weakly curved shell ( $\widehat{\kappa}_\alpha \approx 0$ , for  $\alpha = 1$  and  $2$ ) or cylindrical shell ( $\widehat{\kappa}_2 = 0$ ). It is therefore necessary to categorize shells based on the exact magnitudes of principal curvatures, which will be presented in the subsequent discussions.

Secondly, the material properties involved, such as Young’s modulus and density, also need be non-dimensionalized. As we are investigating shells with multiple layers, the material properties of each layer are compared to those of the bottommost layer

$$E_\mathcal{L} = E_1 \cdot \widehat{E}_\mathcal{L}; \quad \rho_\mathcal{L} = \rho_1 \cdot \widehat{\rho}_\mathcal{L}, \quad (22)$$

where the two introduced quantities  $E_1$  and  $\rho_1$  are the representative Young’s modulus and density of the material assigned to *Layer 1*, respectively.

Thirdly, the non-dimensionalization of certain involved field variables is directly conducted from the traditional plate theory, either based on experimentally summarized axioms (Reissner (1941), Vlasov (1951)) or AA (Zhao et al. (2022)). Consequently, it is found that the displacement components are non-dimensionalized by

$$u_\alpha = \epsilon U \widehat{u}_\alpha, \quad u_3 = U \widehat{u}_3, \quad (23)$$

and the stress field is typically non-dimensionalized by

$$\sigma_{\alpha\beta} = \sigma^* \widehat{\sigma}_{\alpha\beta}; \quad \sigma_{\alpha 3} = \epsilon \sigma^* \widehat{\sigma}_{\alpha 3}; \quad \sigma_{33} = \epsilon^2 \sigma^* \widehat{\sigma}_{33}, \quad (24)$$

where the introduced parameter is chosen to be  $\sigma^* = \frac{\epsilon^2 U E_1}{h}$  according to the non-dimensionalization manipulation of the constitutive law related to the in-plane shear stress  $\sigma_{12}$ . Note that, although the conclusions regarding displacement and stress fields from plate theory are directly applied here, their specific order relationships necessitate further elucidation through comprehensive analyses of shell structures with different magnitudes of principal curvatures.

As partly implied by the dynamic equilibrium equation Eq. (12) and the scaling relations of field quantities Eqs. (23)-(24), the appropriate time-scale is chosen to be

$$t = \epsilon^{m_1} L \sqrt{\frac{\rho_1}{E_1}} \cdot \widehat{t}, \quad (25)$$

where the exponent  $m_1$  is left unspecified until the magnitude of principal curvature against the shell surface dimension  $L$  is determined. Additionally, the prescribed body force vector is non-dimensionalized by

$$\mathbf{f} = \epsilon^{m_2} \frac{U E_1}{h^2} \cdot \widehat{\mathbf{f}}, \quad (26)$$

where similar to Eq. (25), the exponent  $m_2$  remains to be undetermined for the moment. Detailed discussions on the modification of scaling relations of displacement and stress components (Eqs. (23)-(24)), as well as the determination of specific orders of time and body force (Eq. (25)-(26)), will be covered later when investigating shells of different curvature patterns in Secs. 3.3.1 and 3.3.2.

### 3.2. Asymptotic Expansions

To capture the shell behavior in different orders, the asymptotic expansions of the (non-dimensional) displacement and stress fields in terms of the small parameter  $\epsilon$  are first given below

$$\widehat{u}_i \sim \widehat{u}_i^{(0)}(\widehat{\xi}_1, \widehat{\xi}_2, \widehat{\xi}_3) + \epsilon \widehat{u}_i^{(1)}(\widehat{\xi}_1, \widehat{\xi}_2, \widehat{\xi}_3) + \dots; \quad (27a)$$

$$\widehat{\sigma}_{ij} \sim \widehat{\sigma}_{ij}^{(0)}(\widehat{\xi}_1, \widehat{\xi}_2, \widehat{\xi}_3) + \epsilon \widehat{\sigma}_{ij}^{(1)}(\widehat{\xi}_1, \widehat{\xi}_2, \widehat{\xi}_3) + \dots, \quad (27b)$$

where the subindices  $i, j = 1, 2, 3$ ;  $(\widehat{\xi}_1, \widehat{\xi}_2) \in \mathcal{S}$ ,  $\widehat{\xi}_3 \in [-0.5, 0.5]$ .

Based on the previous scaling rules of field variables, the non-dimensional constitutive laws linking the local stress and displacement components are given in detail by

$$\epsilon^2 \widehat{\sigma}_{11} = \frac{\widehat{E}_\mathcal{L}}{(1 + \nu_\mathcal{L})(1 - 2\nu_\mathcal{L})} \left[ \epsilon^2 \frac{1 - \nu_\mathcal{L}}{\widehat{h}_1} \left( \frac{\partial \widehat{u}_1}{\partial \widehat{\xi}_1} + \frac{\widehat{u}_2}{\widehat{h}_2} \frac{\partial \widehat{h}_1}{\partial \widehat{\xi}_2} - \frac{\widehat{\kappa}_1}{\epsilon} \widehat{u}_3 \widehat{a}_1 \right) + \epsilon^2 \frac{\nu_\mathcal{L}}{\widehat{h}_2} \left( \frac{\partial \widehat{u}_2}{\partial \widehat{\xi}_2} + \frac{\widehat{u}_1}{\widehat{h}_1} \frac{\partial \widehat{h}_2}{\partial \widehat{\xi}_1} - \frac{\widehat{\kappa}_2}{\epsilon} \widehat{u}_3 \widehat{a}_2 \right) + \nu_\mathcal{L} \frac{\partial \widehat{u}_3}{\partial \widehat{\xi}_3} \right]; \quad (28a)$$

$$\widehat{\sigma}_{12} = \frac{\widehat{E}_\mathcal{L}}{2(1 + \nu_\mathcal{L})} \left[ \frac{1}{\widehat{h}_1} \left( \frac{\partial \widehat{u}_2}{\partial \widehat{\xi}_1} - \frac{\widehat{u}_2}{\widehat{h}_2} \frac{\partial \widehat{h}_2}{\partial \widehat{\xi}_1} \right) + \frac{1}{\widehat{h}_2} \left( \frac{\partial \widehat{u}_1}{\partial \widehat{\xi}_2} - \frac{\widehat{u}_1}{\widehat{h}_1} \frac{\partial \widehat{h}_1}{\partial \widehat{\xi}_2} \right) \right]; \quad (28b)$$

$$\epsilon^2 \widehat{\sigma}_{22} = \frac{\widehat{E}_\mathcal{L}}{(1 + \nu_\mathcal{L})(1 - 2\nu_\mathcal{L})} \left[ \epsilon^2 \frac{\nu_\mathcal{L}}{\widehat{h}_1} \left( \frac{\partial \widehat{u}_1}{\partial \widehat{\xi}_1} + \frac{\widehat{u}_2}{\widehat{h}_2} \frac{\partial \widehat{h}_1}{\partial \widehat{\xi}_2} - \frac{\widehat{\kappa}_1}{\epsilon} \widehat{u}_3 \widehat{a}_1 \right) + \epsilon^2 \frac{1 - \nu_\mathcal{L}}{\widehat{h}_2} \left( \frac{\partial \widehat{u}_2}{\partial \widehat{\xi}_2} + \frac{\widehat{u}_1}{\widehat{h}_1} \frac{\partial \widehat{h}_2}{\partial \widehat{\xi}_1} - \frac{\widehat{\kappa}_2}{\epsilon} \widehat{u}_3 \widehat{a}_2 \right) + \nu_\mathcal{L} \frac{\partial \widehat{u}_3}{\partial \widehat{\xi}_3} \right]; \quad (28c)$$

$$\epsilon^2 \widehat{\sigma}_{13} = \frac{\widehat{E}_\mathcal{L}}{2(1 + \nu_\mathcal{L})} \left[ \frac{1}{\widehat{h}_1} \left( \frac{\partial \widehat{u}_3}{\partial \widehat{\xi}_1} + \epsilon \widehat{u}_1 \widehat{\kappa}_1 \widehat{a}_1 \right) + \frac{\partial \widehat{u}_1}{\partial \widehat{\xi}_3} \right]; \quad (28d)$$

$$\epsilon^2 \widehat{\sigma}_{23} = \frac{\widehat{E}_\mathcal{L}}{2(1 + \nu_\mathcal{L})} \left[ \frac{1}{\widehat{h}_2} \left( \frac{\partial \widehat{u}_3}{\partial \widehat{\xi}_2} + \epsilon \widehat{u}_2 \widehat{\kappa}_2 \widehat{a}_2 \right) + \frac{\partial \widehat{u}_2}{\partial \widehat{\xi}_3} \right]; \quad (28e)$$

$$\epsilon^4 \widehat{\sigma}_{33} = \frac{\widehat{E}_\mathcal{L}}{(1 + \nu_\mathcal{L})(1 - 2\nu_\mathcal{L})} \left[ \epsilon^2 \frac{\nu_\mathcal{L}}{\widehat{h}_1} \left( \frac{\partial \widehat{u}_1}{\partial \widehat{\xi}_1} + \frac{\widehat{u}_2}{\widehat{h}_2} \frac{\partial \widehat{h}_1}{\partial \widehat{\xi}_2} - \frac{\widehat{\kappa}_1}{\epsilon} \widehat{u}_3 \widehat{a}_1 \right) + \epsilon^2 \frac{\nu_\mathcal{L}}{\widehat{h}_2} \left( \frac{\partial \widehat{u}_2}{\partial \widehat{\xi}_2} + \frac{\widehat{u}_1}{\widehat{h}_1} \frac{\partial \widehat{h}_2}{\partial \widehat{\xi}_1} - \frac{\widehat{\kappa}_2}{\epsilon} \widehat{u}_3 \widehat{a}_2 \right) + (1 - \nu_\mathcal{L}) \frac{\partial \widehat{u}_3}{\partial \widehat{\xi}_3} \right], \quad (28f)$$

where the subindex  $\mathcal{L} = 1, 2, \dots, N$  is recalled to represent the layer index occupied by *Material*  $\mathcal{L}$ .

The original governing equation Eq. (12) can be similarly non-dimensionalized as

$$\begin{aligned} & \epsilon^{-2m_1} \widehat{\rho}_\mathcal{L} \frac{\partial^2 \widehat{u}_1}{\partial \widehat{t}^2} - \epsilon^{m_2-3} \widehat{f}_1 \\ &= \frac{1}{\widehat{h}_1 \widehat{h}_2} \left[ \frac{\partial}{\partial \widehat{\xi}_1} \left( \widehat{h}_2 \widehat{\sigma}_{11} \right) + \frac{\partial}{\partial \widehat{\xi}_2} \left( \widehat{h}_1 \widehat{\sigma}_{12} \right) + \widehat{\sigma}_{12} \frac{\partial \widehat{h}_1}{\partial \widehat{\xi}_2} - \widehat{\sigma}_{22} \frac{\partial \widehat{h}_2}{\partial \widehat{\xi}_1} \right] + \frac{\partial \widehat{\sigma}_{13}}{\partial \widehat{\xi}_3} - \epsilon \frac{2\widehat{\kappa}_1 \widehat{a}_1 \widehat{\sigma}_{13}}{\widehat{h}_1} - \epsilon \frac{\widehat{\kappa}_2 \widehat{a}_2 \widehat{\sigma}_{13}}{\widehat{h}_2}; \end{aligned} \quad (29a)$$

$$\begin{aligned} & \epsilon^{-2m_1} \widehat{\rho}_\mathcal{L} \frac{\partial^2 \widehat{u}_2}{\partial \widehat{t}^2} - \epsilon^{m_2-3} \widehat{f}_2 \\ &= \frac{1}{\widehat{h}_1 \widehat{h}_2} \left[ \frac{\partial}{\partial \widehat{\xi}_1} \left( \widehat{h}_2 \widehat{\sigma}_{12} \right) + \frac{\partial}{\partial \widehat{\xi}_2} \left( \widehat{h}_1 \widehat{\sigma}_{22} \right) + \widehat{\sigma}_{12} \frac{\partial \widehat{h}_2}{\partial \widehat{\xi}_1} - \widehat{\sigma}_{11} \frac{\partial \widehat{h}_1}{\partial \widehat{\xi}_2} \right] + \frac{\partial \widehat{\sigma}_{23}}{\partial \widehat{\xi}_3} - \epsilon \frac{\widehat{\kappa}_1 \widehat{a}_1 \widehat{\sigma}_{23}}{\widehat{h}_1} - \epsilon \frac{2\widehat{\kappa}_2 \widehat{a}_2 \widehat{\sigma}_{23}}{\widehat{h}_2}; \end{aligned} \quad (29b)$$

$$\begin{aligned} & \epsilon^{-2m_1-2} \widehat{\rho}_\mathcal{L} \frac{\partial^2 \widehat{u}_3}{\partial \widehat{t}^2} - \epsilon^{m_2-4} \widehat{f}_3 \\ &= \frac{1}{\widehat{h}_1 \widehat{h}_2} \left[ \frac{\partial}{\partial \widehat{\xi}_1} \left( \widehat{h}_2 \widehat{\sigma}_{13} \right) + \frac{\partial}{\partial \widehat{\xi}_2} \left( \widehat{h}_1 \widehat{\sigma}_{23} \right) \right] + \frac{\partial \widehat{\sigma}_{33}}{\partial \widehat{\xi}_3} - \epsilon \frac{\widehat{\kappa}_1 \widehat{a}_1}{\widehat{h}_1} \left( \widehat{\sigma}_{33} - \frac{1}{\epsilon^2} \widehat{\sigma}_{11} \right) - \epsilon \frac{\widehat{\kappa}_2 \widehat{a}_2}{\widehat{h}_2} \left( \widehat{\sigma}_{33} - \frac{1}{\epsilon^2} \widehat{\sigma}_{22} \right). \end{aligned} \quad (29c)$$

Note that, the terms  $\frac{1}{\widehat{h}_\alpha}$  here denote the inverse of the dimensionless *Lamé coefficients*, which can be further expressed in the form of series expansions, that is,

$$\frac{1}{\widehat{h}_\alpha} = \frac{1}{\widehat{a}_\alpha (1 - \epsilon \widehat{\kappa}_\alpha \widehat{\xi}_3)} = \frac{1}{\widehat{a}_\alpha} \left[ 1 + \epsilon \widehat{\kappa}_\alpha \widehat{\xi}_3 + \left( \epsilon \widehat{\kappa}_\alpha \widehat{\xi}_3 \right)^2 + \dots \right]. \quad (30)$$



### 3.3. Classification of Shell Models with Curvature Patterns

Despite the relative insignificance of the terms  $\epsilon \widehat{\kappa}_\alpha$  in Eqs. (28)-(29) compared to 1, the exact magnitude of  $\widehat{\kappa}_\alpha$  after non-dimensionalization about the shell surface scale  $L$  varies for cases of weakly curved or normally curved shells. These variations result in shifts in the order relations of field variables across different shell types, thereby affecting structural properties such as load-bearing capacity and vibration characteristics. Hence, two specific types of shells (see Fig. 2) corresponding to different curvature patterns are investigated below.

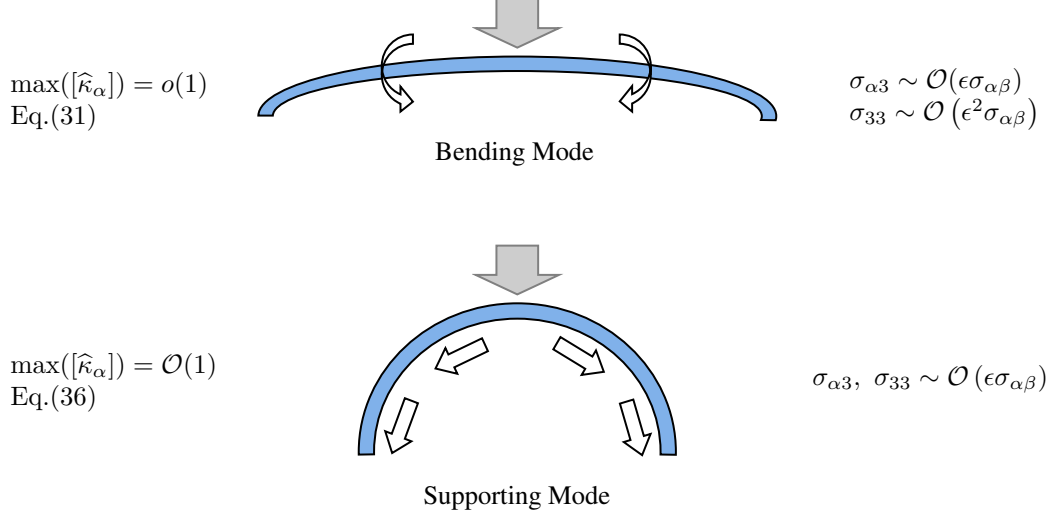


Figure 2: Classification of shells based on the magnitude of maximum dimensionless principal curvature  $\widehat{\kappa}_\alpha$ . The upper panel represents a weakly curved shell, while the lower panel represents a normally curved shell.

#### 3.3.1. Weakly Curved Shell

When the MTS under consideration is nearly flat, as shown in the upper panel of Fig. 2, the maximum curvature of the shell mid-surface is almost imperceptible. Mathematically, we have the following estimation of non-dimensionalized principal curvatures

$$\max([\widehat{\kappa}_\alpha]) = o(1), \quad (31)$$

the symbol “[ $\cdot$ ]” here denotes the set of principal curvatures corresponding to all points investigated on the shell mid-surface  $\mathcal{S}$ .

From the general (non-dimensional) constitutive laws Eq. (28), the local out-plane displacement component is found to be independent of the normal variable in the leading order, i.e.,

$$\widehat{u}_3^{(0)} = \widehat{u}_3^* \left( \widehat{\xi}_1, \widehat{\xi}_2 \right). \quad (32)$$

And with Eqs. (28d) and (28e), the linear relationship between two tangential displacement components at any point inside the investigated MTS and the normal variable  $\widehat{\xi}_3$  is derived

$$\widehat{u}_\alpha^{(0)} \left( \widehat{\xi}_1, \widehat{\xi}_2, \widehat{\xi}_3 \right) = \widehat{u}_\alpha^* \left( \widehat{\xi}_1, \widehat{\xi}_2 \right) - \frac{\widehat{\xi}_3}{\widehat{a}_\alpha} \frac{\partial \widehat{u}_3^* \left( \widehat{\xi}_1, \widehat{\xi}_2 \right)}{\partial \widehat{\xi}_\alpha}, \quad (33)$$

here, the displacement components affiliated with the symbol “\*” represent their counterparts related to the shell mid-surface. Eqs. (32) and (33) coincide with the displacement patterns given by the classical Kirchhoff-Love hypothesis, but only for the leading order. Specifically, for an MTS whose principal curvatures satisfy Eq. (31), the original conclusions regarding the local displacement components  $\widehat{u}_i$  can be retained up to  $\mathcal{O}(\epsilon)$ , that is,

$$\widehat{u}_\alpha^{(d)} \left( \widehat{\xi}_1, \widehat{\xi}_2, \widehat{\xi}_3 \right) = \widehat{u}_\alpha^* \left( \widehat{\xi}_1, \widehat{\xi}_2 \right) - \frac{\widehat{\xi}_3}{\widehat{a}_\alpha} \frac{\partial \widehat{u}_3^{(d)} \left( \widehat{\xi}_1, \widehat{\xi}_2 \right)}{\partial \widehat{\xi}_\alpha}; \quad (34a)$$

$$\widehat{u}_3^{(d)} = \widehat{u}_3^{(d)} \left( \widehat{\xi}_1, \widehat{\xi}_2 \right), \quad (34b)$$

for both  $d = 0$  and  $1$ . And as indicated by the equilibrium equations and constitutive laws, the order relationships of the local displacement and stress fields remain the same as those given by Eqs. (23) and (24).

Following this, as indicated in Sec. 3.1, we will determine the appropriate orders of magnitude for both the observation time  $t$  and the body force vector  $\mathbf{f}$  in the context of weakly curved shell. Given the proximity of the principal curvatures to zero, the influence of in-plane stresses in the equilibrium equation along the thickness direction does not significantly surpass that of the rest transverse components, so that the left end of Eq. (29c) essentially starts from  $\mathcal{O}(1)$ . If the order of the observation time  $m_1 = 0$ , we find at this point that  $\frac{\partial^2 \hat{u}_3^{(d)}}{\partial \hat{t}^2} = 0$ , for  $d = 0, 1$ , suggesting an absence of normal displacement during free vibration—a proposition deemed untenable. Note that, as indicated by Eq. (23), the out-plane displacement  $u_3$  predominates over the in-plane displacement components  $u_\alpha$ , necessitating an extended observation time to discern the vibration modes of the shell in this direction, which is the primary vibration direction during the free vibration of such shells (refer to the thin plate structure as a special case, the free vibration displacement occurs mainly in the direction perpendicular to the midplane). Accordingly, a suitable order here should be  $m_1 = -1$ .

On the other hand, since  $f_i$  ( $i = 1, 2, 3$ ) are all components of the body force vector  $\mathbf{f}$ , these three should be of the same order of magnitude. If the order of  $\mathbf{f}$  is not greater than  $\mathcal{O}(\epsilon^3)$ , i.e.,  $m_2 \leq 3$ , there will be no corresponding stress components to balance with the body force component  $f_3$  in the shell thickness direction. Consequently, as implied by AA, the appropriate order for the body force in this situation is  $m_2 = 4$ .

So far, the values of two unknown parameters in Eqs. (25) and (26) have been determined in this particular case, with  $m_1 = -1$  and  $m_2 = 4$ . By letting  $\epsilon \rightarrow 0$ , Eq. (29) is then simplified to a set of equations where only the one correlated with the thickness direction contains a dimensionless inertial force term and a dimensionless body force term

$$0 = \frac{1}{\hat{a}_1 \hat{a}_2} \left[ \frac{\partial}{\partial \hat{\xi}_1} \left( \hat{a}_2 \hat{\sigma}_{11}^{(0)} \right) + \frac{\partial}{\partial \hat{\xi}_2} \left( \hat{a}_1 \hat{\sigma}_{12}^{(0)} \right) + \hat{\sigma}_{12}^{(0)} \frac{\partial \hat{a}_1}{\partial \hat{\xi}_2} - \hat{\sigma}_{22}^{(0)} \frac{\partial \hat{a}_2}{\partial \hat{\xi}_1} \right] + \frac{\partial \hat{\sigma}_{13}^{(0)}}{\partial \hat{\xi}_3}; \quad (35a)$$

$$0 = \frac{1}{\hat{a}_1 \hat{a}_2} \left[ \frac{\partial}{\partial \hat{\xi}_1} \left( \hat{a}_2 \hat{\sigma}_{12}^{(0)} \right) + \frac{\partial}{\partial \hat{\xi}_2} \left( \hat{a}_1 \hat{\sigma}_{22}^{(0)} \right) + \hat{\sigma}_{12}^{(0)} \frac{\partial \hat{a}_2}{\partial \hat{\xi}_1} - \hat{\sigma}_{11}^{(0)} \frac{\partial \hat{a}_1}{\partial \hat{\xi}_2} \right] + \frac{\partial \hat{\sigma}_{23}^{(0)}}{\partial \hat{\xi}_3}; \quad (35b)$$

$$\hat{\rho}_c \frac{\partial^2 \hat{u}_3^{(0)}}{\partial \hat{t}^2} - \hat{f}_3 = \frac{1}{\hat{a}_1 \hat{a}_2} \left[ \frac{\partial}{\partial \hat{\xi}_1} \left( \hat{a}_2 \hat{\sigma}_{13}^{(0)} \right) + \frac{\partial}{\partial \hat{\xi}_2} \left( \hat{a}_1 \hat{\sigma}_{23}^{(0)} \right) \right] + \frac{\partial \hat{\sigma}_{33}^{(0)}}{\partial \hat{\xi}_3} + \frac{\hat{\kappa}_1}{\epsilon} \hat{\sigma}_{11}^{(0)} + \frac{\hat{\kappa}_2}{\epsilon} \hat{\sigma}_{22}^{(0)}, \quad (35c)$$

from the leading-order dynamic equilibrium equations above, it is obvious that the two inertial forces along the local tangential directions vanish, resulting in a constrained eigenvalue problem when considering free vibration of the shell. One can refer to the works done by Gander et al. (1989) and Ram (2010) for details in obtaining the eigenvalues and corresponding eigenvectors of such a problem. And similar to thin plates, this type of shells primarily resist normal loads through bending deformation (see the upper panel of Fig. 2).

### 3.3.2. Normally Curved Shell

If the maximum principal curvature of an examined point on the shell mid-surface  $\mathcal{S}$  is appreciable, such as spherical ( $\hat{\kappa}_1 = \hat{\kappa}_2 = 1$ ) and cylindrical shells ( $\hat{\kappa}_2 = 0$ ), etc., the order of magnitude of the non-dimensional principal curvatures should satisfy

$$\max([\hat{\kappa}_\alpha]) = \mathcal{O}(1). \quad (36)$$

Based on Eq. (36), further examination of the first two orders of the dimensionless constitutive laws (Eq. (28)) gives the following relations in terms of the in-plane and out-plane displacement components

$$\hat{u}_\alpha^{(0)} = \hat{u}_\alpha^{(0)} \left( \hat{\xi}_1, \hat{\xi}_2 \right); \quad (37a)$$

$$\hat{u}_3^{(0)} = 0; \quad \hat{u}_3^{(1)} = \hat{u}_3^{(1)} \left( \hat{\xi}_1, \hat{\xi}_2 \right), \quad (37b)$$

note also that the trivial leading-order normal displacement (Eq. (37b)) suggests a need for a modification of the originally introduced displacement order relationship (Eq. (23)). Unlike the case of weakly curved

shell presented in Sec. 3.3.1 where the out-plane displacement predominates over the other two, all the three local displacements here are in the same order of magnitude and  $\widehat{u}_3^{(1)}$  actually serves as the normal displacement component corresponding to the shell mid-surface. Thus we have

$$u_\alpha = \epsilon U \left( \widehat{u}_\alpha^{(0)} + \epsilon \widehat{u}_\alpha^{(1)} + \dots \right), \quad u_3 = U \left( \widehat{u}_3^{(0)} + \epsilon \widehat{u}_3^{(1)} + \dots \right) = \epsilon U \left( \widehat{u}_3^{(1)} + \dots \right). \quad (38)$$

The original order relations of the local stress components (Eq. (24)) are also recalibrated for the combined consideration of Eq. (36) and the non-dimensional equilibrium equations Eq. (12). To be specific, the three local transverse stress components  $\sigma_{i3}$ , which are one order higher than the in-plane stresses  $\sigma_{\alpha\beta}$ , should be in the same order of magnitude, that is,

$$\sigma_{\alpha\beta} = \sigma^* \widehat{\sigma}_{\alpha\beta}; \quad \sigma_{i3} = \epsilon \sigma^* \widehat{\sigma}_{i3}. \quad (39)$$

One clarification is warranted here: the leading-order (non-dimensional) transverse shear stresses  $\widehat{\sigma}_{\alpha 3}^{(0)}$  within each layer can be theoretically demonstrated to vary linearly along the thickness direction and to equal to the imposed (non-dimensional) shear forces per area  $\widehat{p}_\alpha$  at the top surface of the MTS  $\mathcal{S}_t$ , i.e.,

$$\widehat{\sigma}_{\alpha 3}^{(0)} = g_\alpha^\mathcal{L} \left( \widehat{\xi}_1, \widehat{\xi}_2 \right) \widehat{\xi}_3 + G_\alpha^\mathcal{L} \left( \widehat{\xi}_1, \widehat{\xi}_2 \right), \quad \text{for } \alpha = 1, 2; \quad \mathcal{L} = 1, \dots, N. \quad (40)$$

The piecewise linear relationship between  $\sigma_{\alpha 3}^{(0)}$  and the thickness coordinate  $\widehat{\xi}_3$  can be partly reflected and justified by Fig. 7, which shows the distribution of the actual transverse shear stresses in a multi-layered spherical shell. And a detailed proof of Eq. (40) will be presented in Appendix A.

Similar to Sec. 3.3.1, here we also need to determine the specific values of  $m_1$  and  $m_2$ . With the appreciable surface curvature, it can be inferred that the terms related to in-plane stress components  $\widehat{\sigma}_{11}$  and  $\widehat{\sigma}_{22}$  in Eq. (29c) are approximately of  $\mathcal{O}(1/\epsilon)$ , which dominate the resistance of the MTS to deformation in the thickness direction. Furthermore, as mentioned above,  $\widehat{u}_3$  starts from the first order ( $\mathcal{O}(\epsilon)$ ). Therefore, the inertial force and body force terms in the dynamic equilibrium equation along the normal direction here are of the same order as those in the other two equations. The specific orders of the observation time and the body force vector are accordingly selected to be  $m_1 = 0$  and  $m_2 = 3$ , respectively.

Without loss of generality, we assume here that both principal curvatures of  $\mathcal{S}$  satisfy Eq. (36), with the spherical shell being one of the special cases. Again, let  $\epsilon \rightarrow 0$ , the non-dimensional governing equations corresponding to normally curved shell are obtained

$$\widehat{\rho}_c \frac{\partial^2 \widehat{u}_1^{(0)}}{\partial \widehat{t}^2} - \widehat{f}_1 = \frac{1}{\widehat{a}_1 \widehat{a}_2} \left[ \frac{\partial}{\partial \widehat{\xi}_1} \left( \widehat{a}_2 \widehat{\sigma}_{11}^{(0)} \right) + \frac{\partial}{\partial \widehat{\xi}_2} \left( \widehat{a}_1 \widehat{\sigma}_{12}^{(0)} \right) + \widehat{\sigma}_{12}^{(0)} \frac{\partial \widehat{a}_1}{\partial \widehat{\xi}_2} - \widehat{\sigma}_{22}^{(0)} \frac{\partial \widehat{a}_2}{\partial \widehat{\xi}_1} \right] + g_1^\mathcal{L} \left( \widehat{\xi}_1, \widehat{\xi}_2 \right); \quad (41a)$$

$$\widehat{\rho}_c \frac{\partial^2 \widehat{u}_2^{(0)}}{\partial \widehat{t}^2} - \widehat{f}_2 = \frac{1}{\widehat{a}_1 \widehat{a}_2} \left[ \frac{\partial}{\partial \widehat{\xi}_1} \left( \widehat{a}_2 \widehat{\sigma}_{12}^{(0)} \right) + \frac{\partial}{\partial \widehat{\xi}_2} \left( \widehat{a}_1 \widehat{\sigma}_{22}^{(0)} \right) + \widehat{\sigma}_{12}^{(0)} \frac{\partial \widehat{a}_2}{\partial \widehat{\xi}_1} - \widehat{\sigma}_{11}^{(0)} \frac{\partial \widehat{a}_1}{\partial \widehat{\xi}_2} \right] + g_2^\mathcal{L} \left( \widehat{\xi}_1, \widehat{\xi}_2 \right); \quad (41b)$$

$$\widehat{\rho}_c \frac{\partial^2 \widehat{u}_3^{(1)}}{\partial \widehat{t}^2} - \widehat{f}_3 = \widehat{\kappa}_1 \widehat{\sigma}_{11}^{(0)} + \widehat{\kappa}_2 \widehat{\sigma}_{22}^{(0)}, \quad (41c)$$

here  $g_\alpha^\mathcal{L} \left( \widehat{\xi}_1, \widehat{\xi}_2 \right)$  are unknown functions of  $\widehat{\xi}_1, \widehat{\xi}_2$  and remain to be solved.

Now we supplement the modifications made in this particular case with some physical elucidations. The body force components here are all of  $\mathcal{O}(\epsilon^3)$ , meaning that the loading capacity of a shell increases with its curvature, which is in line with general intuitions. The order of the time scale in this case,  $m_1 = 0$ , is a higher order quantity than that in Sec. 3.3.1 ( $m_1 = -1$ ). Since the three displacement components in the local coordinate system  $\widehat{u}_i$  are of the same order, the vibration modes along all three directions can be observed simultaneously for a free vibrating shell. So in contrary to Eq. (35), the free vibration problem here corresponds to a complete eigenvalue problem. Furthermore, force balance in the thickness direction (Eq. (41c)) is only determined by the distribution of the in-plane tensions, with the effects of bending stiffness being neglected. As illustrated in the lower panel of Fig. 2, such shells mainly resist normal loads by transmitting forces through in-plane support.

It is also worth noting that AA here effectively determines the order of magnitude of the transverse stresses, which are higher-order quantities compared to the in-plane stresses and are not strictly zero

as suggested by the classical shell hypotheses. Instead they are equal to zero in an asymptotic sense. Once the dominant in-plane stress components are obtained, the transverse stresses can be specified by the integral relations given by Eqs. (35) or (41) (depending on the magnitude of the maximum principal curvature of the investigated shell).

### 3.4. Unified Formulations of Shell Models

Two seemingly disparate deformation modes were discussed in Secs. 3.3.1 and 3.3.2, both of which follow naturally from the process of AA. However, based on the commonalities suggested by the conclusions presented in Sec. 3.3.2, we seek to formulate the two regimes in a unified manner.

The core of the two aforementioned curvature patterns is about the order-determination of the normal displacement and transverse normal stress, i.e.,  $\widehat{u}_3$  and  $\widehat{\sigma}_{33}$ . From Eqs. (34) and (37), the normal displacement of the first two orders are found to be independent of the normal variable  $\widehat{\xi}_3$ , so if we adopt the first-order truncated expression for the normal displacement component of the shell mid-surface, it can automatically degenerate to the corresponding case with a tolerable error when the principal curvatures meet the condition. For this purpose,  $\widehat{u}_3^*$  appearing in Eqs. (32)-(33) and hereafter should take the form

$$\widehat{u}_3^* \left( \widehat{\xi}_1, \widehat{\xi}_2 \right) = \widehat{u}_3^{(0)} \left( \widehat{\xi}_1, \widehat{\xi}_2 \right) + \epsilon \widehat{u}_3^{(1)} \left( \widehat{\xi}_1, \widehat{\xi}_2 \right). \quad (42)$$

The leading-order dominant stress components  $\widehat{\sigma}_{\alpha\beta}^{(0)}$  can be obtained by first eliminating the term  $\partial \widehat{u}_3 / \partial \widehat{\xi}_3$  in Eqs. (28a), (28c) and then taking the limit zero for  $\epsilon$  in the corresponding constitutive equations

$$\widehat{\sigma}_{11}^{(0)} = \frac{\widehat{E}_c}{1 - \nu_c^2} \left( \varepsilon_{11}^{(0)} + \nu_c \varepsilon_{22}^{(0)} \right); \quad (43a)$$

$$\widehat{\sigma}_{12}^{(0)} = \frac{\widehat{E}_c}{2(1 + \nu_c)} \cdot \gamma_{12}^{(0)}; \quad (43b)$$

$$\widehat{\sigma}_{22}^{(0)} = \frac{\widehat{E}_c}{1 - \nu_c^2} \left( \nu_c \varepsilon_{11}^{(0)} + \varepsilon_{22}^{(0)} \right), \quad (43c)$$

where the involved leading-order strain components read

$$\varepsilon_{11}^{(0)} = \frac{1}{\widehat{a}_1} \frac{\partial \widehat{u}_1^{(0)}}{\partial \widehat{\xi}_1} + \frac{\widehat{u}_2^{(0)}}{\widehat{a}_1 \widehat{a}_2} \frac{\partial \widehat{a}_1}{\partial \widehat{\xi}_2} - \frac{\widehat{\kappa}_1}{\epsilon} \left( \widehat{u}_3^{(0)} + \epsilon \widehat{u}_3^{(1)} \right); \quad (44a)$$

$$\varepsilon_{22}^{(0)} = \frac{1}{\widehat{a}_2} \frac{\partial \widehat{u}_2^{(0)}}{\partial \widehat{\xi}_2} + \frac{\widehat{u}_1^{(0)}}{\widehat{a}_1 \widehat{a}_2} \frac{\partial \widehat{a}_2}{\partial \widehat{\xi}_1} - \frac{\widehat{\kappa}_2}{\epsilon} \left( \widehat{u}_3^{(0)} + \epsilon \widehat{u}_3^{(1)} \right); \quad (44b)$$

$$\gamma_{12}^{(0)} = \frac{1}{\widehat{a}_1} \frac{\partial \widehat{u}_2^{(0)}}{\partial \widehat{\xi}_1} + \frac{1}{\widehat{a}_2} \frac{\partial \widehat{u}_1^{(0)}}{\partial \widehat{\xi}_2} - \frac{\widehat{u}_2^{(0)}}{\widehat{a}_1 \widehat{a}_2} \frac{\partial \widehat{a}_2}{\partial \widehat{\xi}_1} - \frac{\widehat{u}_1^{(0)}}{\widehat{a}_1 \widehat{a}_2} \frac{\partial \widehat{a}_1}{\partial \widehat{\xi}_2}. \quad (44c)$$

Substituting Eq. (33) into Eq. (44), all the leading-order in-plane (membrane) strain components can thus be represented by displacements that relate only to the shell mid-surface, that is

$$\varepsilon_{11}^{(0)} = \left( \frac{1}{\widehat{a}_1} \frac{\partial \widehat{u}_1^*}{\partial \widehat{\xi}_1} + \frac{\widehat{u}_2^*}{\widehat{a}_1 \widehat{a}_2} \frac{\partial \widehat{a}_1}{\partial \widehat{\xi}_2} - \frac{\widehat{\kappa}_1}{\epsilon} \widehat{u}_3^* \right) - \widehat{\xi}_3 \left[ \frac{1}{\widehat{a}_1} \frac{\partial}{\partial \widehat{\xi}_1} \left( \frac{1}{\widehat{a}_1} \frac{\partial \widehat{u}_3^*}{\partial \widehat{\xi}_1} \right) + \frac{1}{\widehat{a}_1 \widehat{a}_2^2} \frac{\partial \widehat{a}_1}{\partial \widehat{\xi}_2} \frac{\partial \widehat{u}_3^*}{\partial \widehat{\xi}_2} \right] = \varepsilon_{11}^* + \widehat{\xi}_3 (-k_{11}^*); \quad (45a)$$

$$\varepsilon_{22}^{(0)} = \left( \frac{1}{\widehat{a}_2} \frac{\partial \widehat{u}_2^*}{\partial \widehat{\xi}_2} + \frac{\widehat{u}_1^*}{\widehat{a}_1 \widehat{a}_2} \frac{\partial \widehat{a}_2}{\partial \widehat{\xi}_1} - \frac{\widehat{\kappa}_2}{\epsilon} \widehat{u}_3^* \right) - \widehat{\xi}_3 \left[ \frac{1}{\widehat{a}_2} \frac{\partial}{\partial \widehat{\xi}_2} \left( \frac{1}{\widehat{a}_2} \frac{\partial \widehat{u}_3^*}{\partial \widehat{\xi}_2} \right) + \frac{1}{\widehat{a}_1^2 \widehat{a}_2} \frac{\partial \widehat{a}_2}{\partial \widehat{\xi}_1} \frac{\partial \widehat{u}_3^*}{\partial \widehat{\xi}_1} \right] = \varepsilon_{22}^* + \widehat{\xi}_3 (-k_{22}^*); \quad (45b)$$

$$\begin{aligned} \gamma_{12}^{(0)} &= \left( \frac{1}{\widehat{a}_1} \frac{\partial \widehat{u}_2^*}{\partial \widehat{\xi}_1} + \frac{1}{\widehat{a}_2} \frac{\partial \widehat{u}_1^*}{\partial \widehat{\xi}_2} - \frac{\widehat{u}_2^*}{\widehat{a}_1 \widehat{a}_2} \frac{\partial \widehat{a}_2}{\partial \widehat{\xi}_1} - \frac{\widehat{u}_1^*}{\widehat{a}_1 \widehat{a}_2} \frac{\partial \widehat{a}_1}{\partial \widehat{\xi}_2} \right) - 2 \widehat{\xi}_3 \left( \frac{1}{\widehat{a}_1 \widehat{a}_2} \frac{\partial^2 \widehat{u}_3^*}{\partial \widehat{\xi}_1 \partial \widehat{\xi}_2} - \frac{1}{\widehat{a}_1 \widehat{a}_2^2} \frac{\partial \widehat{a}_2}{\partial \widehat{\xi}_1} \frac{\partial \widehat{u}_3^*}{\partial \widehat{\xi}_2} - \frac{1}{\widehat{a}_1^2 \widehat{a}_2} \frac{\partial \widehat{a}_1}{\partial \widehat{\xi}_2} \frac{\partial \widehat{u}_3^*}{\partial \widehat{\xi}_1} \right) \\ &= \gamma_{12}^* + \widehat{\xi}_3 (-2k_{12}^*), \end{aligned} \quad (45c)$$

here  $\boldsymbol{\varepsilon}^* = \varepsilon_{\alpha\beta} \mathbf{e}_\alpha \otimes \mathbf{e}_\beta$  is the membrane strain tensor associated with the mid-surface  $\mathcal{S}$  of the shell;  $\mathbf{k}^* = -k_{\alpha\beta} \mathbf{e}_\alpha \otimes \mathbf{e}_\beta$  denotes the changes of curvature of the local mid-surface infinitesimal. Therefore,

the dominant stresses obtained in the previous Eq. (43) are able to be further related to these six general strain components of the mid-surface of the MTS, i.e.,

$$\widehat{\sigma}_{11}^{(0)} = \frac{\widehat{E}_\mathcal{L}}{1 - \nu_\mathcal{L}^2} \left[ \varepsilon_{11}^* + \nu_\mathcal{L} \varepsilon_{22}^* + \widehat{\xi}_3 (-k_{11}^*) + \nu_\mathcal{L} \widehat{\xi}_3 (-k_{22}^*) \right]; \quad (46a)$$

$$\widehat{\sigma}_{12}^{(0)} = \frac{\widehat{E}_\mathcal{L}}{2(1 + \nu_\mathcal{L})} \left[ \gamma_{12}^* + \widehat{\xi}_3 (-2k_{12}^*) \right]; \quad (46b)$$

$$\widehat{\sigma}_{22}^{(0)} = \frac{\widehat{E}_\mathcal{L}}{1 - \nu_\mathcal{L}^2} \left[ \nu_\mathcal{L} \varepsilon_{11}^* + \varepsilon_{22}^* + \nu_\mathcal{L} \widehat{\xi}_3 (-k_{11}^*) + \widehat{\xi}_3 (-k_{22}^*) \right]. \quad (46c)$$

### 3.5. Homogenization

It follows that, so far, we have only obtained the corresponding governing equations based on the geometrical and load-bearing characteristics of the MTS, but what we are dealing with remains a three-dimensional equation defined in local curvilinear coordinates, which does not alleviate the complexity of the solving process. Specifically, although only the stress components  $\widehat{\sigma}_{\alpha\beta}^{(0)}$  mentioned above are dominant, the equilibrium of the whole structure is still maintained by all three-dimensional stress components  $\widehat{\sigma}_{ij}^{(0)}$  together, including the dependence of in-plane stresses on the locally complete three curvilinear coordinates  $\widehat{\xi}_i$ ,  $i = 1, 2, 3$ . An intuitive idea is to compress the information about the field functions inside the shell as much as possible into its mid-surface, thus transforming an original three-dimensional problem into one on a two-dimensional manifold.

To this end, homogenization is naturally carried out on local stress fields in the shell thickness direction to generate the stress resultant and stress couple fields, which are defined as follows

- (1) The non-dimensional in-plane stress resultants are the integral of the dominant stress components through the range of the normal variable

$$\widehat{\mathbf{T}} = \widehat{T}_{\alpha\beta} \mathbf{e}_\alpha \otimes \mathbf{e}_\beta; \quad \widehat{T}_{\alpha\beta} = \int_{-\frac{1}{2}}^{\frac{1}{2}} \widehat{\sigma}_{\alpha\beta} d\widehat{\xi}_3. \quad (47)$$

- (2) The non-dimensional stress resultants of transverse shear stresses are the integral of the corresponding stress components with respect to the normal coordinate  $\widehat{\xi}_3$

$$\widehat{N}_\alpha = \int_{-\frac{1}{2}}^{\frac{1}{2}} \widehat{\sigma}_{\alpha 3} d\widehat{\xi}_3. \quad (48)$$

- (3) The stress couples are the through-the-thickness integral of the first-order moments of three dominant in-plane stresses

$$\widehat{\mathbf{M}} = \widehat{M}_{\alpha\beta} \mathbf{e}_\alpha \otimes \mathbf{e}_\beta; \quad \widehat{M}_{\alpha\beta} = \int_{-\frac{1}{2}}^{\frac{1}{2}} \widehat{\sigma}_{\alpha\beta} \widehat{\xi}_3 d\widehat{\xi}_3. \quad (49)$$

In addition the  $m$ -th moment of a piece-wise constant function defined in the interval  $(-\frac{1}{2}, \frac{1}{2})$  is introduced to facilitate the subsequent derivation, and the expression is written by

$$\langle A_\mathcal{L} \rangle_m = \sum_{\mathcal{L}=1}^N A_\mathcal{L} \int_{\widehat{\xi}_3^\mathcal{L}}^{\widehat{\xi}_3^{\mathcal{L}+1}} (\widehat{\xi}_3)^m d\widehat{\xi}_3, \quad (50)$$

here the interval  $(\widehat{\xi}_3^\mathcal{L}, \widehat{\xi}_3^{\mathcal{L}+1})$  denotes the dimensionless thickness range of *Layer*  $\mathcal{L}$ .

Now we set about deriving the reduced two-dimensional governing equations of the investigated MTS. First, integrating the leading order of Eq. (29) with respect to  $\widehat{\xi}_3$  over the interval  $(-\frac{1}{2}, \frac{1}{2})$  yields

$$\epsilon^{-2m_1} \widehat{\mathcal{T}}_1^I - \epsilon^{m_2-3} \widehat{f}_1 = \frac{1}{\widehat{a}_1 \widehat{a}_2} \left[ \frac{\partial}{\partial \widehat{\xi}_1} \left( \widehat{a}_2 \widehat{T}_{11}^{(0)} \right) + \frac{\partial}{\partial \widehat{\xi}_2} \left( \widehat{a}_1 \widehat{T}_{12}^{(0)} \right) + \widehat{T}_{12}^{(0)} \frac{\partial \widehat{a}_1}{\partial \widehat{\xi}_2} - \widehat{T}_{22}^{(0)} \frac{\partial \widehat{a}_2}{\partial \widehat{\xi}_1} \right] + \widehat{p}_1; \quad (51a)$$

$$\epsilon^{-2m_1} \widehat{\mathcal{T}}_2^I - \epsilon^{m_2-3} \widehat{f}_2 = \frac{1}{\widehat{a}_1 \widehat{a}_2} \left[ \frac{\partial}{\partial \widehat{\xi}_1} \left( \widehat{a}_1 \widehat{T}_{12}^{(0)} \right) + \frac{\partial}{\partial \widehat{\xi}_2} \left( \widehat{a}_1 \widehat{T}_{22}^{(0)} \right) + \widehat{T}_{12}^{(0)} \frac{\partial \widehat{a}_2}{\partial \widehat{\xi}_1} - \widehat{T}_{11}^{(0)} \frac{\partial \widehat{a}_1}{\partial \widehat{\xi}_2} \right] + \widehat{p}_2; \quad (51b)$$

$$\epsilon^{-2m_1-2} \widehat{\mathcal{T}}_3^I - \epsilon^{m_2-4} \widehat{f}_3 = \frac{1}{\widehat{a}_1 \widehat{a}_2} \left[ \frac{\partial}{\partial \widehat{\xi}_1} \left( \widehat{a}_2 \widehat{N}_1^{(0)} \right) + \frac{\partial}{\partial \widehat{\xi}_2} \left( \widehat{a}_1 \widehat{N}_2^{(0)} \right) \right] + \frac{\widehat{\kappa}_1}{\epsilon} \widehat{T}_{11}^{(0)} + \frac{\widehat{\kappa}_2}{\epsilon} \widehat{T}_{22}^{(0)} + \widehat{p}_3, \quad (51c)$$

where the superscript ‘‘I’’ here implies that the corresponding variable relates to the inertial force, and the new introduced notations  $\widehat{\mathcal{T}}_i^I$  represent the homogenized inertial force components, whose specific definitions are given below

$$\widehat{\mathcal{T}}_i^I = \sum_{\mathcal{L}=1}^N \int_{\widehat{\xi}_3^{\mathcal{L}}}^{\widehat{\xi}_3^{\mathcal{L}+1}} \widehat{\rho}_{\mathcal{L}} \ddot{u}_i d\widehat{\xi}_3 = \langle \widehat{\rho}_{\mathcal{L}} \rangle_0 \frac{\partial^2 \widehat{u}_i^*}{\partial \widehat{t}^2} + \langle \widehat{\rho}_{\mathcal{L}} \rangle_1 \frac{\partial^2 \widehat{\varphi}_i^*}{\partial \widehat{t}^2}, \quad (52)$$

where  $\langle \cdot \rangle_m$ ,  $m = 0, 1$ , take the definition of Eq. (50). The term  $\frac{\partial^2 \widehat{\mathbf{u}}^*}{\partial \widehat{t}^2} = \left[ \frac{\partial^2 \widehat{u}_1^*}{\partial \widehat{t}^2}, \frac{\partial^2 \widehat{u}_2^*}{\partial \widehat{t}^2}, \frac{\partial^2 \widehat{u}_3^*}{\partial \widehat{t}^2} \right]^T$  represents the dimensionless acceleration vector, and  $\frac{\partial^2 \widehat{\boldsymbol{\varphi}}^*}{\partial \widehat{t}^2} = \left[ -\frac{1}{\widehat{a}_1} \frac{\partial \widehat{u}_3^*}{\partial \widehat{\xi}_1}, -\frac{1}{\widehat{a}_2} \frac{\partial \widehat{u}_3^*}{\partial \widehat{\xi}_2}, 0 \right]^T$  represents the dimensionless angular acceleration vector.

Note that Eq. (51c) contains the transverse shear stress resultants  $\widehat{N}_{\alpha}^{(0)}$ , which actually account for the out-plane effects, so in order to obtain a set of fully two-dimensional governing equations, another equation related to the stress couples  $\widehat{M}_{\alpha\beta}^{(0)}$  should be determined. Here the leading order of Eqs. (29a) and (29b) are multiplied by the normal coordinate  $\widehat{\xi}_3$ , and their corresponding first-order moments are then given by

$$\epsilon^{-2m_1} \widehat{\mathcal{M}}_1^I = \frac{1}{\widehat{a}_1 \widehat{a}_2} \left[ \frac{\partial}{\partial \widehat{\xi}_1} \left( \widehat{a}_2 \widehat{M}_{11}^{(0)} \right) + \frac{\partial}{\partial \widehat{\xi}_2} \left( \widehat{a}_1 \widehat{M}_{12}^{(0)} \right) + \widehat{M}_{12}^{(0)} \frac{\partial \widehat{a}_1}{\partial \widehat{\xi}_2} - \widehat{M}_{22}^{(0)} \frac{\partial \widehat{a}_2}{\partial \widehat{\xi}_1} \right] - \widehat{N}_1 + \frac{\widehat{p}_1}{2}; \quad (53a)$$

$$\epsilon^{-2m_1} \widehat{\mathcal{M}}_2^I = \frac{1}{\widehat{a}_1 \widehat{a}_2} \left[ \frac{\partial}{\partial \widehat{\xi}_1} \left( \widehat{a}_1 \widehat{M}_{12}^{(0)} \right) + \frac{\partial}{\partial \widehat{\xi}_2} \left( \widehat{a}_1 \widehat{M}_{22}^{(0)} \right) + \widehat{M}_{12}^{(0)} \frac{\partial \widehat{a}_2}{\partial \widehat{\xi}_1} - \widehat{M}_{11}^{(0)} \frac{\partial \widehat{a}_1}{\partial \widehat{\xi}_2} \right] - \widehat{N}_2 + \frac{\widehat{p}_2}{2}, \quad (53b)$$

likewise, the notations  $\widehat{\mathcal{M}}_i^I$  here represent the homogenized inertial force moments, which are defined by

$$\widehat{\mathcal{M}}_i^I = \sum_{\mathcal{L}=1}^N \int_{\widehat{\xi}_3^{\mathcal{L}}}^{\widehat{\xi}_3^{\mathcal{L}+1}} \widehat{\rho}_{\mathcal{L}} \ddot{u}_i \widehat{\xi}_3 d\widehat{\xi}_3 = \langle \widehat{\rho}_{\mathcal{L}} \rangle_1 \frac{\partial^2 \widehat{u}_i^*}{\partial \widehat{t}^2} + \langle \widehat{\rho}_{\mathcal{L}} \rangle_2 \frac{\partial^2 \widehat{\varphi}_i^*}{\partial \widehat{t}^2}. \quad (54)$$

Combined with Eq. (51c), the terms regarding  $\widehat{N}_{\alpha}^{(0)}$  can be eliminated, thus resulting in a relation between the leading-order stress couples  $\widehat{M}_{\alpha\beta}^{(0)}$ , i.e.,

$$\begin{aligned} & \frac{1}{\widehat{a}_1 \widehat{a}_2} \left\{ \frac{\partial}{\partial \widehat{\xi}_1} \left( \frac{\widehat{a}_2 \partial \widehat{M}_{11}^{(0)}}{\widehat{a}_1 \partial \widehat{\xi}_1} \right) + \frac{\partial}{\partial \widehat{\xi}_2} \left( \frac{\widehat{a}_1 \partial \widehat{M}_{22}^{(0)}}{\widehat{a}_2 \partial \widehat{\xi}_2} \right) + \frac{\partial}{\partial \widehat{\xi}_1} \left[ \frac{(\widehat{M}_{11}^{(0)} - \widehat{M}_{22}^{(0)}) \partial \widehat{a}_2}{\widehat{a}_1 \partial \widehat{\xi}_1} \right] + \frac{\partial}{\partial \widehat{\xi}_2} \left[ \frac{(\widehat{M}_{22}^{(0)} - \widehat{M}_{11}^{(0)}) \partial \widehat{a}_1}{\widehat{a}_2 \partial \widehat{\xi}_2} \right] \right\} \\ & + 2 \frac{\partial^2 \widehat{M}_{12}^{(0)}}{\partial \widehat{\xi}_1 \partial \widehat{\xi}_2} + \frac{\partial}{\partial \widehat{\xi}_1} \left( \frac{2 \widehat{M}_{12}^{(0)} \partial \widehat{a}_1}{\widehat{a}_1 \partial \widehat{\xi}_2} \right) + \frac{\partial}{\partial \widehat{\xi}_2} \left( \frac{2 \widehat{M}_{12}^{(0)} \partial \widehat{a}_2}{\widehat{a}_2 \partial \widehat{\xi}_1} \right) \left\} + \frac{\widehat{\kappa}_1 \widehat{T}_{11}^{(0)}}{\epsilon} + \frac{\widehat{\kappa}_2 \widehat{T}_{22}^{(0)}}{\epsilon} + \frac{1}{2} \frac{\partial (\widehat{a}_2 \widehat{p}_1)}{\partial \widehat{\xi}_1} + \frac{1}{2} \frac{\partial (\widehat{a}_1 \widehat{p}_2)}{\partial \widehat{\xi}_2} + \widehat{p}_3 = \\ & \epsilon^{-2m_1-2} \widehat{\mathcal{T}}_3^I + \epsilon^{-2m_1} \frac{\partial}{\partial \widehat{\xi}_1} \left( \widehat{a}_2 \widehat{\mathcal{M}}_1^I \right) + \epsilon^{-2m_1} \frac{\partial}{\partial \widehat{\xi}_2} \left( \widehat{a}_1 \widehat{\mathcal{M}}_2^I \right) - \epsilon^{m_2-4} \widehat{f}_3. \end{aligned} \quad (55)$$

So far, Eqs. (51a), (51b) and (55) together constitute the homogenized dynamic equilibrium equations of the MTS, which are a set of equations containing the in-plane stress resultants and couples (both just functions of the in-plane dominant stress components  $\widehat{\sigma}_{\alpha\beta}^{(0)}$ ). Based on the specific expressions of the leading-order in-plane stress components Eq. (46), the involved homogenized quantities defined by Eqs. (47) and (49) can be expressed by

$$\widehat{T}_{\alpha\beta}^{(0)} = \mathcal{A}_{\alpha\beta\gamma\lambda} \varepsilon_{\gamma\lambda}^* + \mathcal{B}_{\alpha\beta\gamma\lambda} (-k_{\gamma\lambda}^*); \quad (56a)$$

$$\widehat{M}_{\alpha\beta}^{(0)} = \mathcal{B}_{\alpha\beta\gamma\lambda} \varepsilon_{\gamma\lambda}^* + \mathcal{D}_{\alpha\beta\gamma\lambda} (-k_{\gamma\lambda}^*), \quad (56b)$$

where the introduced material matrices are actually the different order moments of the original elasticity matrix, that is,

$$\mathcal{A}_{\alpha\beta\gamma\lambda} = \langle \mathbb{C}_{\alpha\beta\gamma\lambda} \rangle_0; \quad \mathcal{B}_{\alpha\beta\gamma\lambda} = \langle \mathbb{C}_{\alpha\beta\gamma\lambda} \rangle_1; \quad \mathcal{D}_{\alpha\beta\gamma\lambda} = \langle \mathbb{C}_{\alpha\beta\gamma\lambda} \rangle_2, \quad (57)$$

it can be found that, in a physical sense, the matrices  $\mathcal{A}$ ,  $\mathcal{D}$  and  $\mathcal{B}$  capture the local extensional, bending and coupling effects of the shell mid-surface infinitesimal, respectively. Similar to what has been pointed

out in the work of [Reissner & Stavsky \(1961\)](#) on heterogeneous anisotropic laminated plates and that of [Zhao & Zhu \(2023\)](#) on thin microstructural plates, these three also possess certain symmetry in their indices. For isotropic cases, we have

$$\mathcal{A}_{\alpha\beta\gamma\lambda} = \mathcal{A}_{\beta\alpha\gamma\lambda} = \mathcal{A}_{\gamma\lambda\alpha\beta}; \quad \mathcal{B}_{\alpha\beta\gamma\lambda} = \mathcal{B}_{\beta\alpha\gamma\lambda} = \mathcal{B}_{\gamma\lambda\alpha\beta}; \quad \mathcal{D}_{\alpha\beta\gamma\lambda} = \mathcal{D}_{\beta\alpha\gamma\lambda} = \mathcal{D}_{\gamma\lambda\alpha\beta}. \quad (58)$$

#### 4. Model Implementation in an Isogeometric Manner

In the preceding sections, our focus has been on theoretically deriving the asymptotic formulations of laminated shell structures. However, to systematically analyze these structures, specific numerical implementations are necessary. In this paper, the isogeometric discretization is adopted for the simulation process due to the fact that the non-uniform rational B-spline (NURBS) basis function is able to provide smoothness of any order ( $C^\infty$ -continuity) across elements while presenting an accurate description of complex surfaces. And these properties prove particularly advantageous in the rotation-free Kirchhoff-Love shell models ([Kiendl et al. \(2009\)](#), [Nguyen-Thanh et al. \(2011\)](#), [Kiendl et al. \(2015\)](#)), where at least  $C^1$ -continuity is required for the approximate basis functions.

##### 4.1. The NURBS Surfaces and Reparametrization

As indicated, the original geometric representation of the shell mid-surface Eq. (1) can be alternatively achieved by means of NURBS surfaces in the form of

$$\mathbf{r}(\xi_1, \xi_2) = \sum_{i=1}^n \sum_{j=1}^m R_{i,j}^{p,q}(\xi_1, \xi_2) \mathbf{P}_{i,j}, \quad (59)$$

where  $\xi_1, \xi_2$  are the NURBS parameters, as illustrated in Fig. 3.  $\mathbf{P}_{i,j}$  represents a vector comprising the coordinates of  $n \times m$  control points in the  $\xi_1$ -parameter and  $\xi_2$ -parameter directions, while  $R_{i,j}^{p,q}$  stand for the NURBS basis functions (piecewise rational polynomials), with  $p, q$  denoting the degrees of the corresponding B-spline basis functions. For further insights into the mathematics behind the NURBS surfaces, one may refer to the work of [Piegl & Tiller \(1997\)](#).

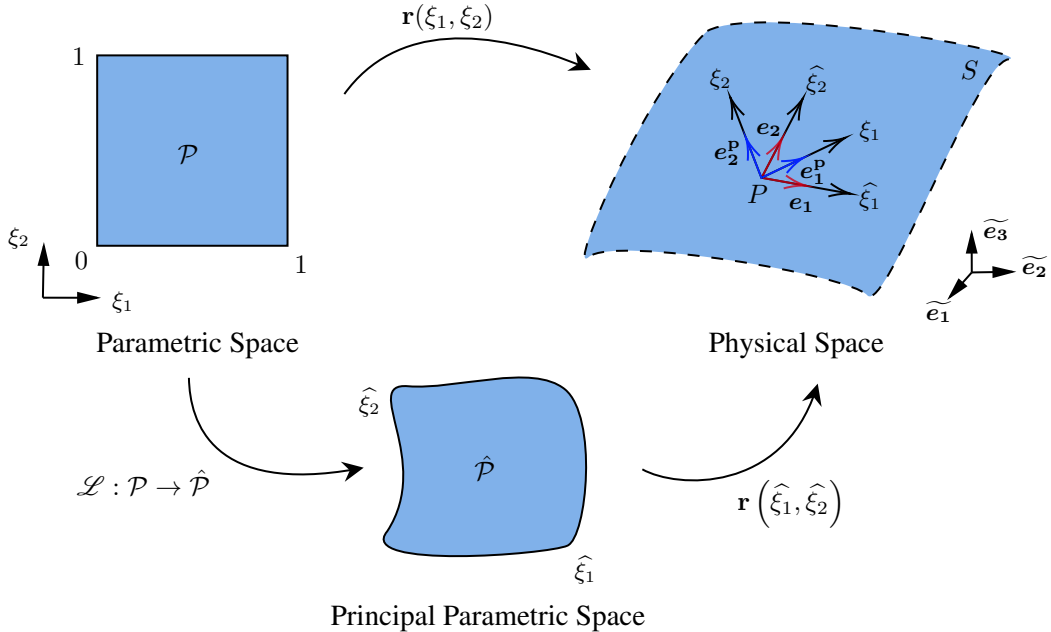


Figure 3: Illustration of the mapping relationship between the NURBS parametric space  $\mathcal{P}$  and shell mid-surface in the physical space  $\mathcal{S}$ . The one-to-one mapping  $\mathcal{L} : \mathcal{P} \rightarrow \hat{\mathcal{P}}$  defines a reparametrization for the representation of shell mid-surface, which bridges the gap between the principal-parameter-based analysis and the NURBS-based computation.

Note that a new set of surface parameters  $(\xi_1, \xi_2)$  has been introduced with the adoption of the NURBS representation Eq. (59), which generally differ from the coordinates  $(\hat{\xi}_1, \hat{\xi}_2)$  employed in formulating the equations of the MTS outlined in Secs. 2 and 3. This is because, mathematically, a set of surface parameters constitutes a mesh coinciding with the principal curvature network of the surface if and only

if they satisfy the aforementioned diagonal condition, i.e., Eq. (3). Hence, the NURBS parameters  $(\xi_1, \xi_2)$  used for generating the geometry do not necessarily parameterize the “lines of curvature” of the surface, as indicated in red and blue in Fig. 3, the tangent vectors  $(\mathbf{e}_1^p, \mathbf{e}_2^p)$  associated with the NURBS parameters may not align with those  $(\mathbf{e}_1, \mathbf{e}_2)$  associated with the principal parameters.

By choosing the “lines of curvature” as parametric curves, the characteristics of various shell types are more straightforward to interpret, and the derivation of stress-strain relations appears to be simpler and more direct, which has already been demonstrated by Reissner (1941).

Given all these advantages, why bother with reparametrization? Here are the two main reasons. Firstly, for the mid-surface geometry described by Eq. (59), the calculation of derivatives of the surface with respect to NURBS parameters is straightforward, whereas that based on the principal parameters presents some unwanted complexities. Additionally, when working with basis vectors  $(\mathbf{e}_1, \mathbf{e}_2)$ , special boundary conditions (e.g., symmetry boundaries, etc.) are not easy to handle, which is not an issue if it is considered in the parameter directions  $(\mathbf{e}_1^p, \mathbf{e}_2^p)$  or more directly, in the global Cartesian coordinate  $(\tilde{\mathbf{e}}_1, \tilde{\mathbf{e}}_2, \tilde{\mathbf{e}}_3)$ . As a consequence, the partial derivatives originally taken with respect to the principal parameters  $\hat{\xi}_\alpha$  should be transformed to those in terms of the NURBS parameters  $\xi_\alpha$ . Moreover, the displacement components in the local orthogonal curvilinear coordinate system have to be transformed into the global Cartesian coordinate system to facilitate the numerical implementation, such as the imposition of boundary conditions and the avoidance of stress singularities caused by isolated umbilical points.

Let  $\mathcal{L} : (\xi_1, \xi_2) \rightarrow (\hat{\xi}_1, \hat{\xi}_2)$  be a one-to-one regular map, whose expression is given by

$$\hat{\xi}_\alpha = \hat{\xi}_\alpha(\xi_1, \xi_2), \quad (60)$$

thus defining a reparametrization for the shell mid-surface:  $\mathbf{r} = \mathbf{r}(\hat{\xi}_1(\xi_1, \xi_2), \hat{\xi}_2(\xi_1, \xi_2))$ . The mapping relationship between two sets of tangent vectors of the surface at a particular point  $P$ , e.g., the principal directions  $\mathbf{r}_{\hat{\xi}_\alpha}$  and the parameter directions  $\mathbf{r}_{\xi_\alpha}$ , can be obtained by the chain rule, that is,

$$\mathbf{r}_{\hat{\xi}_\beta} = \frac{\partial \xi_\alpha}{\partial \hat{\xi}_\beta} \cdot \mathbf{r}_{\xi_\alpha}, \quad (61)$$

the Einstein summation convention is adopted here. From differential geometry, the principal direction corresponds to the eigenvector of the *Weingarten map*, and  $\partial \xi_\alpha / \partial \hat{\xi}_\beta$  actually serve as the combination coefficients for two parameter vectors  $\mathbf{r}_{\xi_\alpha}$ .

Once the mapping relation is obtained, the partial derivatives in the original shell governing equations (Eqs. (51a), (51b) and (55)) and the strain-displacement relations (Eq. (45)) can be transformed into derivatives with respect to the NURBS parameter coordinates  $(\xi_1, \xi_2)$  through the same coefficients as in Eq. (61), i.e.,

$$(\cdot)_{,\hat{\xi}_\beta} = J_{\alpha\beta} \cdot (\cdot)_{,\xi_\alpha}, \quad (62)$$

for simplicity, the mapping Jacobian  $[\partial \xi_\alpha / \partial \hat{\xi}_\beta]$  is denoted by  $J$  hereafter.

#### 4.2. Variational Formulation and Isogeometric Discretization

For the numerical implementation of shell equations, we start this section from the principle of virtual work, which states the equilibrium of internal and external virtual work under any admissible variation, i.e.,  $\delta W = \delta W_{\text{int}} - \delta W_{\text{ext}} = 0$ . Mathematically, this is given by

$$\delta W(\mathbf{u}, \delta \mathbf{u}) = \left. \frac{d}{dt} \right|_{t=0} W(\mathbf{u} + t \delta \mathbf{u}) := D_{\delta \mathbf{u}} W(\mathbf{u}) = 0, \quad \delta \mathbf{u} \in \mathcal{V}, \quad (63)$$

here the operator  $D_{\delta \mathbf{u}}$  is known as the Gâteaux derivative. The test function space  $\mathcal{V} = \{v | v \in H^2(\Omega); v = 0, \text{ on } \partial_u \Omega\}$  and  $H^2(\Omega)$  denotes the Sobolev space, where the function elements should be square-integrable up to the second derivatives, i.e.,  $H^2(\Omega) = \{v | D^\alpha v \in L^2(\Omega), |\alpha| \leq 2\}$ , with the notation  $D^\alpha = \frac{\partial^{|\alpha|}}{\partial x_1^{\alpha_1} \dots \partial x_n^{\alpha_n}}$ ,  $|\alpha| = \sum_{i=1}^n \alpha_i$ .



Since two parametric coordinates are involved here, as shown in Fig. 3, the global-to-local transformation should be taken into account when investigating the specific variational formulation. For an MTS, the leading-order internal virtual work is defined by

$$\begin{aligned}\delta W_{\text{int}}^0 &= \int_{\Omega} [\boldsymbol{\sigma} : \delta \boldsymbol{\varepsilon} + \rho_{\mathcal{L}} \ddot{\mathbf{u}} \cdot \delta \mathbf{u}]_{\tilde{u}_i} \, d\Omega \\ &= \int_{\widehat{\mathcal{P}}} [\mathbf{T} : \delta \boldsymbol{\varepsilon}^* + \mathbf{M} : \delta \mathbf{k}^* + \boldsymbol{\mathcal{T}}^I \cdot \delta \mathbf{u}^* + \boldsymbol{\mathcal{M}}^I \cdot \delta \boldsymbol{\varphi}^*]_{u_i^*} \Big|_{J_{\Omega \rightarrow (\widehat{\mathcal{P}} \times \widehat{\xi}_3)}} \Big|_{d\widehat{\mathcal{P}}} \quad (64) \\ &= \int_{\mathcal{P}} [\mathbf{T} : \delta \boldsymbol{\varepsilon}^* + \mathbf{M} : \delta \mathbf{k}^* + \boldsymbol{\mathcal{T}}^I \cdot \delta \mathbf{u}^* + \boldsymbol{\mathcal{M}}^I \cdot \delta \boldsymbol{\varphi}^*]_{\tilde{u}_i^*} \Big|_{J_{\Omega \rightarrow (\mathcal{P} \times \xi_3)}} \Big|_{d\mathcal{P}},\end{aligned}$$

and the leading-order external virtual work is defined by

$$\begin{aligned}\delta W_{\text{ext}}^0 &= \int_{\Omega} [\mathbf{f} \cdot \delta \mathbf{u}]_{\tilde{u}_i} \, d\Omega + \int_{\partial_t \Omega} [\mathbf{p} \cdot \delta \mathbf{u}]_{\tilde{u}_i} \, d\mathcal{S}_t \\ &= \int_{\widehat{\mathcal{P}}} [\mathbf{f} \cdot \delta \mathbf{u}^*]_{u_i^*} \Big|_{J_{\Omega \rightarrow (\widehat{\mathcal{P}} \times \widehat{\xi}_3)}} \Big|_{d\widehat{\mathcal{P}}} + \int_{\widehat{\mathcal{P}}} \left[ \mathbf{p} \cdot \left( \delta \mathbf{u}^* + \frac{1}{2} \delta \boldsymbol{\varphi}^* \right) \right]_{u_i^*} \Big|_{J_{\partial_t \Omega \rightarrow \widehat{\mathcal{P}}}} \Big|_{d\widehat{\mathcal{P}}} \quad (65) \\ &= \int_{\mathcal{P}} [\mathbf{f} \cdot \delta \mathbf{u}^*]_{\tilde{u}_i^*} \Big|_{J_{\Omega \rightarrow (\mathcal{P} \times \xi_3)}} \Big|_{d\mathcal{P}} + \int_{\mathcal{P}} \left[ \mathbf{p} \cdot \left( \delta \mathbf{u}^* + \frac{1}{2} \delta \boldsymbol{\varphi}^* \right) \right]_{\tilde{u}_i^*} \Big|_{J_{\partial_t \Omega \rightarrow \mathcal{P}}} \Big|_{d\mathcal{P}},\end{aligned}$$

where the subscript outside the square bracket indicates the specific variables of the functions contained within the brackets.  $\tilde{u}_i$ ,  $u_i^*$ , and  $\tilde{u}_i^*$  are identified as the displacement components in the Cartesian coordinate system, along the local principal directions within the mid-surface, and along the global coordinate axes within the mid-surface, respectively. Therefore, we have the following relationship

$$\mathbf{u} = \tilde{u}_i \tilde{\mathbf{e}}_i; \quad \mathbf{u}^* = u_i^* \mathbf{e}_i = \tilde{u}_i^* \tilde{\mathbf{e}}_i. \quad (66)$$

where  $\mathbf{u}$  and  $\mathbf{u}^*$  represent the displacement field and that of the shell mid-surface  $\mathcal{S}$ . The third identities of Eqs. (64) and (65) denote the local-to-global displacement transformation with an intention of avoiding the difficulties and singularities introduced by the isolated umbilical point, which is inherent in the surface geometry such as the ellipsoidal surface.

Some remarks regarding the main variables involved in the above equations are summarized as follows. The in-plane stress resultant tensor  $\mathbf{T}$  and the stress couple tensor  $\mathbf{M}$  can be obtained simply by re-dimensionalizing Eq. (56), and the expressions for the corresponding virtual membrane strain  $\delta \boldsymbol{\varepsilon}^*$  and the changes of curvature  $\delta \mathbf{k}^*$  are obtained by first multiplying Eq. (45) by the coefficient  $\frac{hU}{L^2}$  and then taking the variation. Furthermore,  $\boldsymbol{\mathcal{T}}^I$  and  $\boldsymbol{\mathcal{M}}^I$  stand for the thickness-averaged inertial force and moment vectors, respectively, whose non-dimensional expressions are given in Eqs. (52) and (54).  $\delta \mathbf{u}^*$  and  $\delta \boldsymbol{\varphi}^*$  here denote the (mid-surface) virtual displacement and the virtual rotation angle of the normal, their expressions are written by

$$\delta \mathbf{u}^* = [\delta u_1^*, \delta u_2^*, \delta u_3^*]^T; \quad (67a)$$

$$\delta \boldsymbol{\varphi}^* = \left[ -\frac{h}{a_1} \frac{\partial (\delta u_3^*)}{\partial \widehat{\xi}_1}, -\frac{h}{a_2} \frac{\partial (\delta u_3^*)}{\partial \widehat{\xi}_2}, 0 \right]^T. \quad (67b)$$

The Jacobian determinant involved in Eq. (64) satisfies:  $|J_{\Omega \rightarrow (\mathcal{P} \times \xi_3)}| = |J_{\Omega \rightarrow (\widehat{\mathcal{P}} \times \widehat{\xi}_3)}| |J_{\widehat{\mathcal{P}} \rightarrow \mathcal{P}}|$ , which measures the volume change of a volume infinitesimal from the physical space  $\Omega$  to the NURBS parametric space  $(\mathcal{P} \times \xi_3)$ , and  $|J_{\partial_t \Omega \rightarrow \mathcal{P}}| = |J_{\partial_t \Omega \rightarrow \widehat{\mathcal{P}}}| |J_{\widehat{\mathcal{P}} \rightarrow \mathcal{P}}|$  in Eq. (65) measures the area ratio between the actual surface  $\partial_t \Omega \subseteq \mathcal{S}_t$ , on which the surface force  $\mathbf{t}$  is imposed, and its counterpart in the NURBS parametric space  $\mathcal{P}$ . The specific expressions for several Jacobian determinants mentioned above will be derived in Appendix B.

Up to this point, the weak forms have been presented pertaining to the so-called strong forms of the boundary value problem defined by Eqs. (17)-(19), (51a)-(51b) and (55). However, for the sake of numerical implementation, an appropriate discretization approach should be adopted to further convert the weak form Eq. (63), or equivalently Eqs. (64)-(65), into a system of linear algebraic equations. In the context of shell problems, the isogeometric discretization is deemed ‘‘appropriate’’ due to its capacity to

facilitate straightforward calculation of the second derivatives contained in the changes of curvature  $\mathbf{k}^*$ , while circumventing the need for additional rotational degrees of freedom.

In this way, the displacement field  $\mathbf{u}^*$  of the mid-surface, as well as the virtual displacement field  $\delta\mathbf{u}^*$ , is discretized by directly applying the NURBS basis functions  $R_{i,j}^{p,q}$ , which characterize the geometry (Eq. (59)), to the shape functions that approximate the solution fields, i.e.,

$$\mathbf{u}^*(\xi_1, \xi_2, t) = \sum_{l=1}^{n_{\text{cp}}^e} R_l(\xi_1, \xi_2) \mathbf{u}_l^e(t) \Rightarrow \mathbf{u}^* = \mathbf{R} \cdot \mathbf{u}^e; \quad (68a)$$

$$\delta\mathbf{u}^*(\xi_1, \xi_2, t) = \sum_{l=1}^{n_{\text{cp}}^e} R_l(\xi_1, \xi_2) \delta\mathbf{u}_l^e(t) \Rightarrow \delta\mathbf{u}^* = \mathbf{R} \cdot \delta\mathbf{u}^e, \quad (68b)$$

where  $n_{\text{cp}}^e$  denotes the total number of control points in an element  $\mathcal{S}^e$ , and  $\mathbf{u}_l^e$  is the element nodal displacement vector at the  $l$ -th control point, with its components corresponding to the global Cartesian coordinates. And one can refer to Eqs. (C.7) and (C.8) for the specific expressions of the NURBS basis function matrix  $\mathbf{R}$ , also known as the shape function matrix, and the element nodal displacement vector  $\mathbf{u}^e$ .

Based on the discretized nodal displacement vector provided by Eq. (68), the integrands of the internal and external virtual work can be re-expressed in matrix forms, and notably, both strain and acceleration terms within an element, along with their variations, can be related to displacements of the shell mid-surface  $\mathbf{u}^*$ , which are further expressed by the corresponding nodal displacements  $\mathbf{u}_l^e$  ( $l = 1, \dots, n_{\text{cp}}^e$ ) of the element control points. With all relevant variables now discretized and presented in matrix forms, we can finally show the linear algebraic equations through the discretized form of the principle of virtual work. Generally, such equations can be expressed either in global form as  $\mathbf{M}\ddot{\mathbf{u}}^n + \mathbf{K}\mathbf{u}^n = \mathbf{F}$  or in the discretized form of elements as:

$$\sum_{e=1}^{\text{nel}} (\mathbf{M}^e \ddot{\mathbf{u}}^e + \mathbf{K}^e \mathbf{u}^e = \mathbf{F}^e), \quad (69)$$

where “nel” denotes the total number of elements  $\mathcal{S}^e$ , and  $\mathbf{u}^e$  is the nodal displacement vector of all control points in an element. The summation operation refers to the assembly process of elements. Therefore, the corresponding global matrices and vectors are formed by  $\mathbf{M} = \sum_{e=1}^{\text{nel}} (\mathbf{M}^e)$ ,  $\mathbf{K} = \sum_{e=1}^{\text{nel}} (\mathbf{K}^e)$ ,  $\mathbf{F} = \sum_{e=1}^{\text{nel}} (\mathbf{F}^e)$  and  $\mathbf{u}^n = \sum_{e=1}^{\text{nel}} (\mathbf{u}^e)$ .

Next, we present the specific expressions for the element mass and stiffness matrix and the nodal force vector in Eq. (69). They are

$$\mathbf{M}^e = \int_{\mathcal{P}^e} \mathbf{N}^T \mathbf{P}^e \mathbf{N} |J_{\Omega \rightarrow (\mathcal{P} \times \xi_3)}| d\mathcal{P}; \quad (70a)$$

$$\mathbf{K}^e = \int_{\mathcal{P}^e} \mathbf{B}^T \mathbf{D}^e \mathbf{B} |J_{\Omega \rightarrow (\mathcal{P} \times \xi_3)}| d\mathcal{P}; \quad (70b)$$

$$\mathbf{F}^e = \int_{\mathcal{P}^e} [\mathbf{R}^T \mathbf{Q}^T \mathbf{f}^e |J_{\Omega \rightarrow (\mathcal{P} \times \xi_3)}| + \mathbf{R}^T \mathbf{Q}^T \mathbf{p}^e |J_{\partial_t \Omega \rightarrow \mathcal{P}}|] d\mathcal{P}. \quad (70c)$$

Brief explanations of the quantities involved in the above equations need to be included here. In Eq. (70a),  $\mathbf{N}$  is the augmented shape function matrix connecting the nodal displacements  $\mathbf{d}^l$  and the displacement-rotation vector  $\left[ (\mathbf{u}^*)^T, (\boldsymbol{\varphi}^*)^T \right]^T$ , and  $\mathbf{P}^e$  represents the element density matrix. For the stiffness matrix  $\mathbf{K}^e$  defined by Eq. (70b),  $\mathbf{B}$  is the strain-displacement matrix, and  $\mathbf{D}^e$  denotes a new elasticity matrix consisting of the extensional, coupling and bending stiffness  $\mathbf{A}$ ,  $\mathbf{B}$  and  $\mathbf{D}$ , whose components are presented in Eq. (57). Finally, in Eq. (70c),  $\mathbf{R}$  represents the shape function matrix as shown in Eq. (68), and  $\mathbf{Q}$  is an orthogonal matrix enabled by the relationship of displacement components under two coordinate systems, i.e.,  $u_i^*$  and  $\tilde{u}_i^*$  in Eq. (66). Two vectors  $\mathbf{f}^e$  and  $\mathbf{p}^e$  correspond to the body and surface forces imposed on the element control points, respectively. The detailed expressions of the related matrices and vectors can be found in Appendix C.

## 5. Numerical Validations

Based on the previous theoretical derivation, several numerical examples will be covered in this section to demonstrate the reliability of the proposed isogeometric-based asymptotic framework. The specific

numerical implementation of the asymptotic expressions of the MTS presented in Secs. 3 and 4 are carried out on the MATLAB<sup>®</sup> R2022b platform with several related IGA functions provided by Du et al. (2020), and the obtained results are further validated by checking their deviations from those computed by direct numerical simulation based on the COMSOL Multiphysics<sup>®</sup> v. 5.6. (2020). In this particular section, the modified shell obstacle course, i.e., (1) Pinched cylinder with end diaphragms (Fig. 4(a)), (2) Scordelis-Lo roof (Fig. 4(b)) and (3) Pinched hemisphere with a 18° hole (Fig. 4(c)), are included first to evaluate the performance of the asymptotic formulations for multi-layered shells. Then we focus on the role of the external shear forces, displacement and stress fields under shear deformations are given here in the absence of the SCF and assumed displacement expressions. Moreover, the approximate errors regarding the increase of shell thickness, as well as free vibration problems, is considered to assess the current framework.

### 5.1. Shell Obstacle Course

Three benchmark problems, as shown in Fig. 4, are considered in this section to assess the performance of the proposed shell element under complex strain states. Note that, the original problems devised by Belytschko et al. (1985) and Macneal & Harder (1985) are modified to three-layered shells with the thickness proportions of  $\lambda_1 = \lambda_3 = 0.35$ ,  $\lambda_2 = 0.3$ . The basic information is presented on the top-left of each panel of Fig. 4. We here study the vertical displacement of three prescribed points A, B and C, their specific values are compared with the results obtained from fine-mesh FEA and related studies are also carried out to check the convergence performance with the refinement of the discretized mesh.

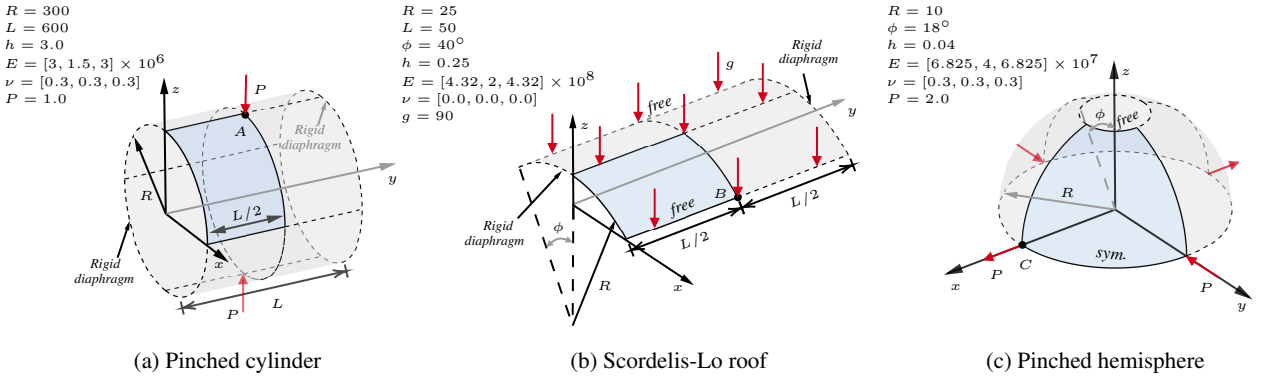


Figure 4: Illustration of the mid-surface geometries and boundary conditions of the modified shell obstacle course for three-layered thin shells. (a) pinched cylinder with two ends attached to rigid diaphragms; (b) scordelis-lo roof subject to a dead weight of 90 per unit area; (c) pinched hemisphere with a 18° hole. Only the blue parts are considered here due to the intrinsic symmetry of the shell geometries and the particular boundary conditions.

For simplicity, only one eighth of the cylindrical and hemispherical shell, and a quarter of the Scordelis-Lo roof, refer to the blue parts in Fig. 4, will be modeled owing to the symmetric nature of the shell geometry and their imposed boundary conditions. Fig. 5 shows the convergence behavior of the proposed method in three obstacle problems. We can find that, all three cases present good convergence behavior corresponding to the reference line obtained from the fine-mesh FEA, with relative errors roughly of  $\mathcal{O}(\epsilon)$ .

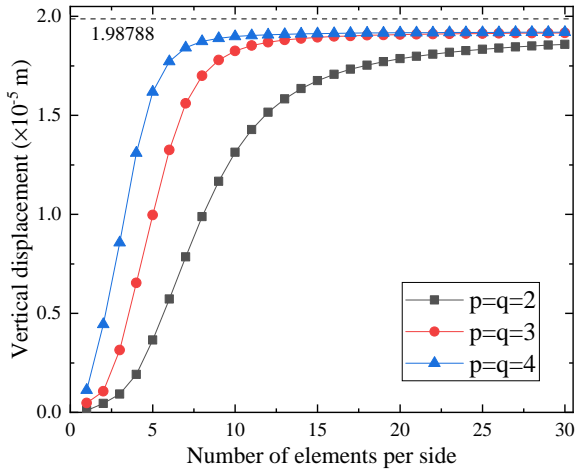
### 5.2. Undamped Free Vibration

We then investigate the mode and angular frequency of the MTS under the case of free vibration. It has been proved in Sec. 3.3.1 that, free vibration of the weakly curved shell actually corresponds to a constrained eigenvalue problem, which resembles the behavior of thin plates. For normally curved shells, as shown by Eq. (41), all three inertial forces participate in the governing equations. To obtain the general eigenvalue problem of this case, the field solution is firstly written as follows

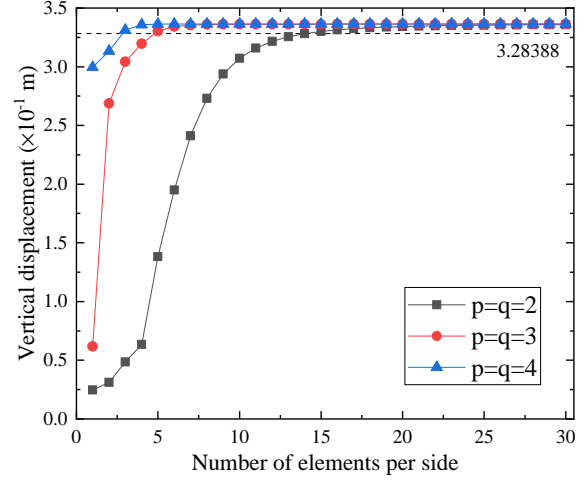
$$\mathbf{u}^e(\xi_1, \xi_2, t) = \mathbf{U}^e(\xi_1, \xi_2) \sin(\omega t + \phi), \quad (71)$$

where  $\mathbf{U}^e$  represents the element mode shape vector and  $\omega$  is called the angular (circular) frequency. Substituting Eq. (71) into the discretized governing equations (Eq. (69)) and setting  $\mathbf{F}^e = \mathbf{0}$  due to undamped vibration, the eigenvalue problem is finally expressed by

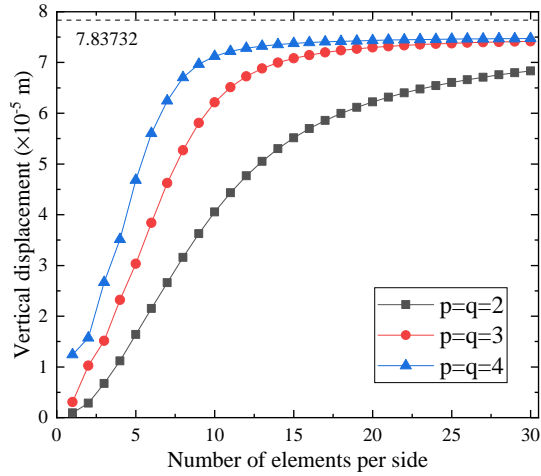
$$\mathbf{K}\mathbf{U} = \omega^2\mathbf{M}\mathbf{U}, \quad (72)$$



(a) Pinched cylinder: Convergence study of  $u_3^A$



(b) Scordelis-Lo roof: Convergence study of  $u_3^B$



(c) Pinched hemisphere: Convergence study of  $u_1^C$

Figure 5: Convergence study for the modified shell obstacle course shown in Fig. 4. The p-refinement is carried out by choosing the NURBS basis functions with degrees  $p = q = 2, 3, 4$ . The h-refinement is achieved by increasing the number of elements per side. And the horizontal dashed line represents the reference value obtained from fine-mesh FEA with 3D solid elements.

Table 1: Comparison of the first eight angular frequency  $\omega$  (rad/s) for the free vibration of hemispherical and cylindrical three-layered shells.

$\epsilon = h/L$	Method	Mode Sequence							
		1	2	3	4	5	6	7	8
(a) One-eighth cylindrical shell shown in Fig. 4(a)									
0.1	Present Method	0.0249	0.0378	0.0622	0.0748	0.0777	0.0778	0.0847	0.1071
	Fine-mesh	0.0240	0.0345	0.0622	0.0706	0.0723	0.0764	0.0785	0.1063
	Relative Error (%)	4.06	9.56	0.00	5.95	7.53	1.82	7.92	0.77
0.01	Present Method	0.0089	0.0090	0.0139	0.0212	0.0219	0.0241	0.0268	0.0278
	Fine-mesh	0.0087	0.0090	0.0137	0.0210	0.0219	0.0239	0.0267	0.0275
	Relative Error (%)	2.28	1.00	1.67	1.21	0.05	0.82	0.41	0.97
(b) One-eighth spherical shell shown in Fig. 4(c)									
0.1	Present Method	12.4083	17.9600	22.3795	25.3521	26.4880	34.0364	36.5192	36.8108
	Fine-mesh	11.8187	17.8066	21.6047	24.5352	25.7001	31.8979	34.4589	34.7435
	Relative Error (%)	4.99	0.86	3.59	3.33	3.07	6.70	5.98	5.95
0.01	Present Method	2.8879	12.9907	17.6279	18.5418	21.4444	21.8301	21.9999	22.5321
	Fine-mesh	2.8322	12.8322	17.6262	18.5360	21.4363	21.8221	21.9874	22.5152
	Relative Error (%)	1.97	1.24	0.00	0.03	0.04	0.04	0.06	0.08

from which the angular frequency for undamped free vibration of shells can be obtained. And  $\mathbf{U} = \sum_{e=1}^{\text{nel}} (\mathbf{U}^e)$  is the corresponding global mode shape vector.

In this section, we consider the free vibration behavior of two types of shells, three-layered cylindrical shells with end diaphragms and spherical shells with a  $18^\circ$  hole. The material density of each layer is selected to be  $\rho_\ell = [7800, 5000, 7800]$  kg/m<sup>3</sup> from bottom to top. The small parameter  $\epsilon$  takes two values 0.1 and 0.01 for both cases, while the remaining geometry and material parameters are the same as those listed in Fig. 4.

Table. 1 shows the first eight angular frequency  $\omega$  for two types of shells and aspect ratios. The values obtained based on the derived asymptotic expressions are compared to those given by the fine-mesh FEA, and we can find that, the proposed method based on AA exhibits a good accuracy in capturing the angular frequency of the free vibration of the MTS, and the accuracy increases as MTS becomes thinner (from  $\epsilon = 0.1$  to  $\epsilon = 0.01$ ).

### 5.3. Transverse Shear Stresses in Normally Curved Shells

For normally curved shells whose maximum non-dimensional principal curvature satisfies Eq. (36), the leading-order transverse stress components in each layer have been proved to be linear functions of the normal variable  $\hat{\xi}_3$  (Eq. (40)). In this section, we consider an eighth of a multi-layered spherical shell, as shown in the blue part of Fig. 6. Two external shear forces  $p_1 = 5000$  N/m<sup>2</sup> and  $p_2 = 8000$  N/m<sup>2</sup> are applied on the top surface of the shell. In order to justify Eq. (40) from a fully computational aspect, we devise to extract the local transverse shear stresses given by the fine-mesh FEA along the surface normal at point D ( $(\xi_1, \xi_2) = (0.5, 0.5)$ ) and then check the actual variation of  $\sigma_{\alpha 3}$  in the shell thickness direction.

The variations of  $\sigma_{\alpha 3}$  obtained from direct analysis with extremely fine mesh about the shell thickness coordinate are presented in Fig. 7 for shells with 1 to 4 layers. We can find that, Figs. 7(b)-7(d) all show a piecewise linear distribution along the thickness direction and the turning points of the slopes are exactly located at the junctions of different layers, i.e., the value of the vertical dashed line correspond to the location of the interface, which can be obtained from the thickness ratio  $\lambda_\ell$  presented in Fig. 6. Based on the theoretical derivation, the distribution of  $\sigma_{\alpha 3}$  in a shell with a single layer can be approximated by a straight line simply connecting the top and bottom surfaces to the values of the applied shear forces. Note that, there is a deviation between the actual transverse shear stress and the linear relationship given by AA in Fig. 7(a), as well as some localized fluctuations observed in Figs. 7(b)-7(d). These can be considered as the correction effects of higher-order terms, while the trends of  $\sigma_{\alpha 3}$  in the MTS have been well captured by the leading-order relationships (Eq. (40)).

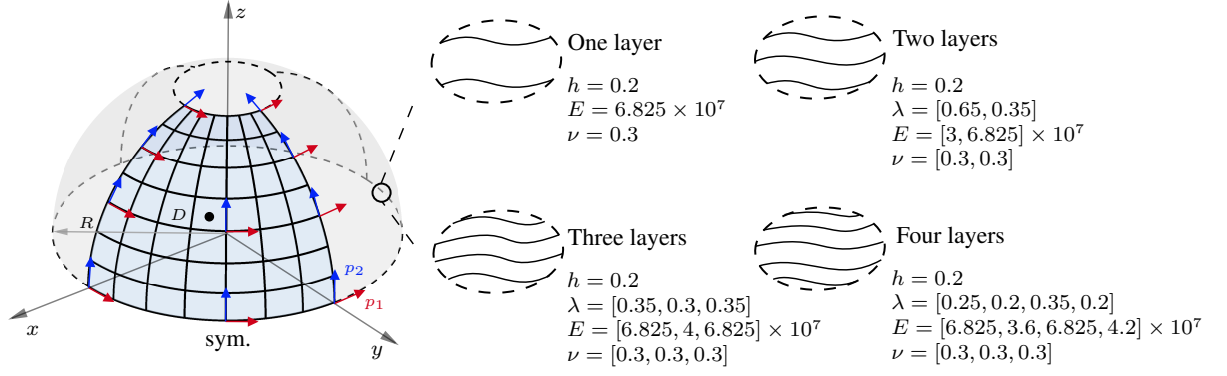
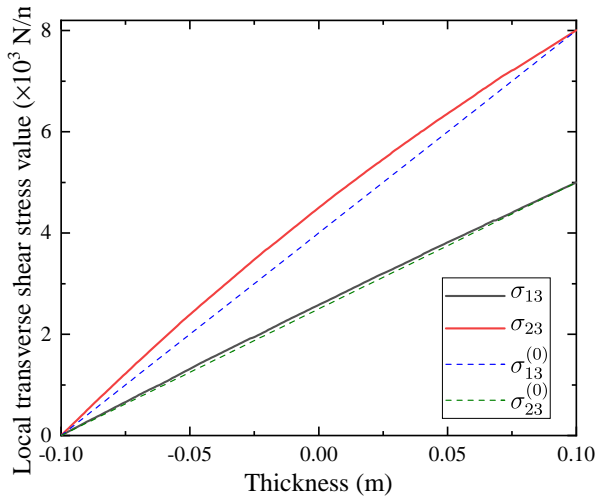
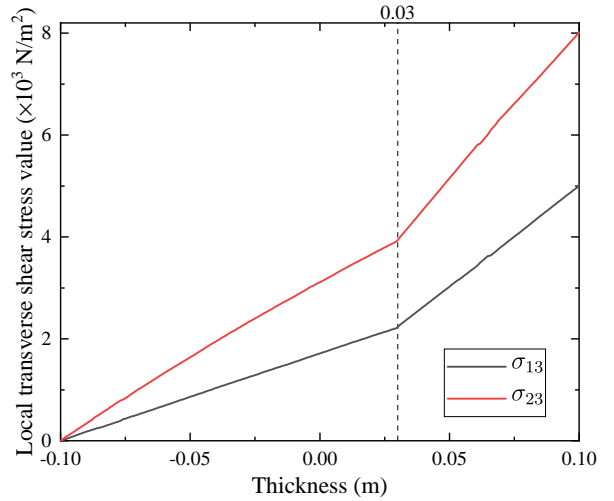


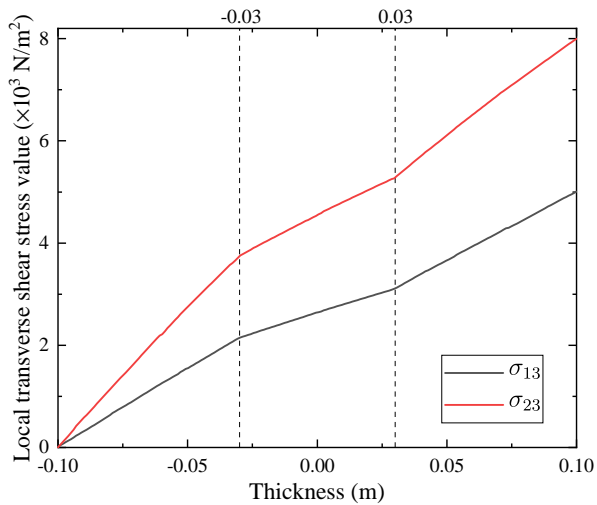
Figure 6: Illustration of the mid-surface of a multi-layered spherical shell with a  $18^\circ$  hole at each pole. Its radius is selected to be  $R = 4$ . The applied shear forces point in a set of orthogonal principal directions with magnitudes  $p_1 = 5000 \text{ N/m}^2$  and  $p_2 = 8000 \text{ N/m}^2$ , respectively. The right four panels present the parameters needed for modeling shells with different layers  $\mathcal{L} = 1, 2, 3, 4$ . Due to the symmetry of shell geometry and loading conditions, only one eighth of the structure (gridded part) is modeled here.



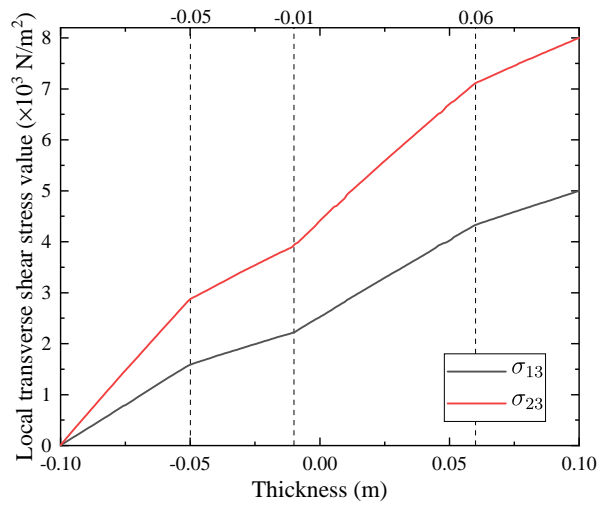
(a) Variation of  $\sigma_{\alpha 3}$  in one-layered spherical shell



(b) Variation of  $\sigma_{\alpha 3}$  in two-layered spherical shell



(c) Variation of  $\sigma_{\alpha 3}$  in three-layered spherical shell



(d) Variation of  $\sigma_{\alpha 3}$  in four-layered spherical shell

Figure 7: Variation of the transverse shear stress components  $\sigma_{\alpha 3}$  obtained from fine-mesh FEA along the shell thickness.

Table 2: Specific values for surface loads corresponding to different thicknesses. The thickness ratios of layers from bottom to top are  $\lambda = [0.35, 0.3, 0.35]$ , the Young’s moduli are  $E = [6.825, 4, 6.825] \times 10^7$  Pa, the Poisson’s ratios are  $\nu = [0.3, 0.3, 0.3]$ , and the radius of the mid-surface is fixed at  $R = 4$  m.

Shell thickness	$\epsilon = h/R$	Surface shear $p_1$ (N/m <sup>2</sup> )	Surface shear $p_2$ (N/m <sup>2</sup> )	Surface pressure $p_3$ (N/m <sup>2</sup> )
0.04	0.01	0	60	1
0.08	0.02	0	540	12
0.12	0.03	0	$1.8 \times 10^3$	60
0.16	0.04	0	$4.2 \times 10^3$	$1.7 \times 10^2$
0.20	0.05	0	$8 \times 10^3$	$5 \times 10^2$
0.24	0.06	0	$1 \times 10^4$	$8.5 \times 10^2$
0.28	0.07	0	$2 \times 10^4$	$1.5 \times 10^3$
0.32	0.08	0	$3 \times 10^4$	$2.5 \times 10^3$
0.36	0.09	0	$4 \times 10^4$	$4 \times 10^3$
0.40	0.10	0	$6 \times 10^4$	$5 \times 10^3$
0.50	0.125	0	$1 \times 10^5$	$1.5 \times 10^4$

#### 5.4. The Thinness Assumption and the Role of Applied Shear Forces

In engineering, a shell is typically regarded as “thin” if the condition  $\max(h/R) \leq 0.05$  is satisfied. As the ratio increases, the influence of transverse shear stress becomes increasingly significant and cannot be neglected, rendering the traditional Kirchhoff-Love hypothesis inapplicable to such “thick shells”. However, the aforementioned inequality actually circumscribes a rather rough boundary between thin and thick shells, which raises questions about the necessity of classifying shells strictly based on their thickness. The main concerns are twofold: first, whether the relative error of the model becomes unacceptable once the thickness ratio exceeds 0.05, and second, whether it is necessary to account for the transverse shear stress in shells subjected to shear deformation. And in the following, we will elucidate these two aspects through numerical examples.

##### 5.4.1. Theory Applicability to Various Aspect Ratios

We here first test the applicability of the present theory to multi-layered shells of various thicknesses. For three-layered spherical shells, specific values for the layer proportions, Young’s moduli, and Poisson’s ratios are provided in Fig. 6. The mid-surface radius of the shell is fixed at  $R = 4$  m with the thickness varying in the range  $t \in [0.04, 0.5]$  m. As demonstrated by the scaling relations of the stress field (Eq. (24)), the orders-of-magnitude of the applied surface loads  $\mathbf{p}$  should vary accordingly. For clarity, the specific parameter settings for each case are listed below in Table. 2.

Fig. 8 illustrates the variation in the maximum relative error between simulations of three-layer spherical shell deformations using the proposed method and the results from fine-mesh FEA across the above 11 different thickness scenarios. The dashed line here represents a commonly-accepted boundary of aspect ratio for a shell to be regarded as “thin”, i.e.,  $\epsilon = 0.05$ . From the figure, we observe that the accuracy of the model decreases with an increasing shell thickness-radius ratio. However, multi-layered shells with a thickness ratio even up to 0.08 can still be modeled and analyzed using the “geometrical thinness” assumption if maximum relative errors of approximately 7% in displacement and 10% in stress fields are considered acceptable. Additionally, the errors here should also include the potential effects of boundary layer (BL), which will be specifically discussed in Sec. 5.4.2.

##### 5.4.2. Multi-layered Shells with Applied Surface Shear Loads

For the second aspect, we aim to examine the role of the applied surface shear forces and the corresponding transverse shear stresses from a more rational perspective within the present framework proposed in this paper. The CST is believed to be unreasonable due to a pre-assumed trivial transverse strain state when the investigated MTS undergoes shear deformation. So the common practice is to introduce a SCF  $K$  based on the FSDT to compensate for the transverse shear stresses that are uniformly distributed along the thickness, or to resort to the HOTs. However, several issues may occur for the consideration of multi-layered shell structures. First, determining the exact SCF  $K$  for laminated/layered shells with complex cross-sections is not an easy task (Gruttmann & Wagner (2017)). Second, higher-order kinematic expressions in the HOTs are mainly axiom-based and lack rational support. Here in this section, we will present the deformation responses of different types of shells subject to shear forces, including

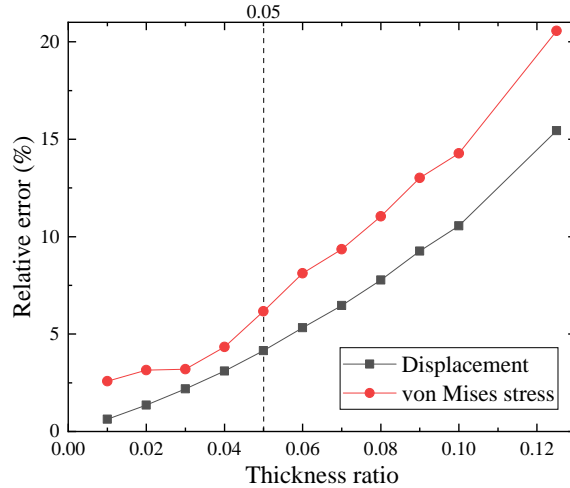


Figure 8: Relative errors between the displacement and stress fields provided by the present framework and those from the fine mesh FEA with respect to the aspect ratio  $\epsilon = h/R$  of a three-layered spherical shell as shown in Fig. 6. The vertical dashed line ( $\epsilon = 0.05$ ) here represents a widely-accepted boundary between thin shells and thick shells.

spherical shells, cylindrical shells, and more generally, ellipsoidal shells. The obtained displacement and stress fields are further compared to those computed based on the 3D solid element FEA, which serve as benchmarks during our validation process.

A three-layer spherical shell with a mid-surface radius of 4 m and a overall thickness of 0.2 m subject to a given shear force is first considered here. The thickness ratio of each layer is selected to be  $\lambda = [0.35, 0.3, 0.35]$  from bottom to top, the corresponding Young’s moduli and Poisson’s ratios are  $E = [6.825, 4, 6.825] \times 10^7$  Pa and  $\nu = [0.3, 0.3, 0.3]$ , respectively. The shear force is imposed on the upper surface of the spherical shell, with the magnitudes of its components along two principal directions being  $p_1 = 5000$  N/m<sup>2</sup> and  $p_2 = 8000$  N/m<sup>2</sup>. Only half of the structure is modeled here, so the symmetric boundary condition is used for the lower boundary (refer to the specific geometry shown in Fig. 6).

Fig. 9 shows the contour plots of one half of the considered spherical shell, including the magnitudes of the displacement and von Mises stress fields and their corresponding results given by the benchmarks (fine-mesh FEA). The maximum relative error of the displacement field is 14.65% at point (1.2361, 0, 3.8042) m and that of the von Mises stress field is 96.45% at point (0.9095, 0.8371, 3.8042) m. Note that these two particular positions are located at the free boundary of the MTS, as indicated by the red diamond marks in Figs. 9(b) and 9(d), where the largest deviations in displacement and von Mises stress are concentrated. This is mainly due to the “BL effects”. A BL is a thin region that contains a large strain energy gradient (Lee & Bathe (2002)) and is generally believed to be responsible for failures in predictions of traditional models, which are valid for regions far from the structural boundary. General treatments regarding the BL have been discussed in the works of Howell et al. (2008) for linear plates and Green (1962) for thin elastic shells. They both successfully derived equations for the BL effects, which finally leading to the change in the boundary conditions on such boundaries without having to solve them explicitly. Therefore, since the BL effects are not of our major concern for the time being, the average relative error is adopted here as a new measure of the model accuracy. Specifically,  $80 \times 80$  data points are selected uniformly, and their corresponding relative errors with the benchmarks are calculated and then averaged.

In this way, the averaged relative error for the displacement is 7.30% and that for the von Mises stress is 5.95%, which are both roughly of  $\mathcal{O}(\epsilon)$ . The present framework thus exhibits a good accuracy in modeling multi-layered spherical shells under shear deformation (except for the BL regions) without the need to introduce additional problem-dependent SCF or intuition-based displacement patterns.

Next we consider a three-layered cylindrical shell of thickness  $h = 15$  m, subjected to a shear force  $\mathbf{p} = (300, 400, 0)$  N/m<sup>2</sup> applied to the top surface of the shell. The other geometric parameters, material properties, as well as the boundary conditions for the investigated cylindrical shell are the same as those presented in Fig. 4(a). The maximum relative errors of displacement and von Mises stress occur at points (288.4197, 0, 82.5475) m and (0, 0, 300) m, as shown by the red diamonds marked in Figs. 10(b) and 10(d). This demonstrates that the BL effects are also significant in the vicinity of fixed boundaries (or boundaries attached to rigid diaphragms). In this case, the averaged relative errors for the displacement



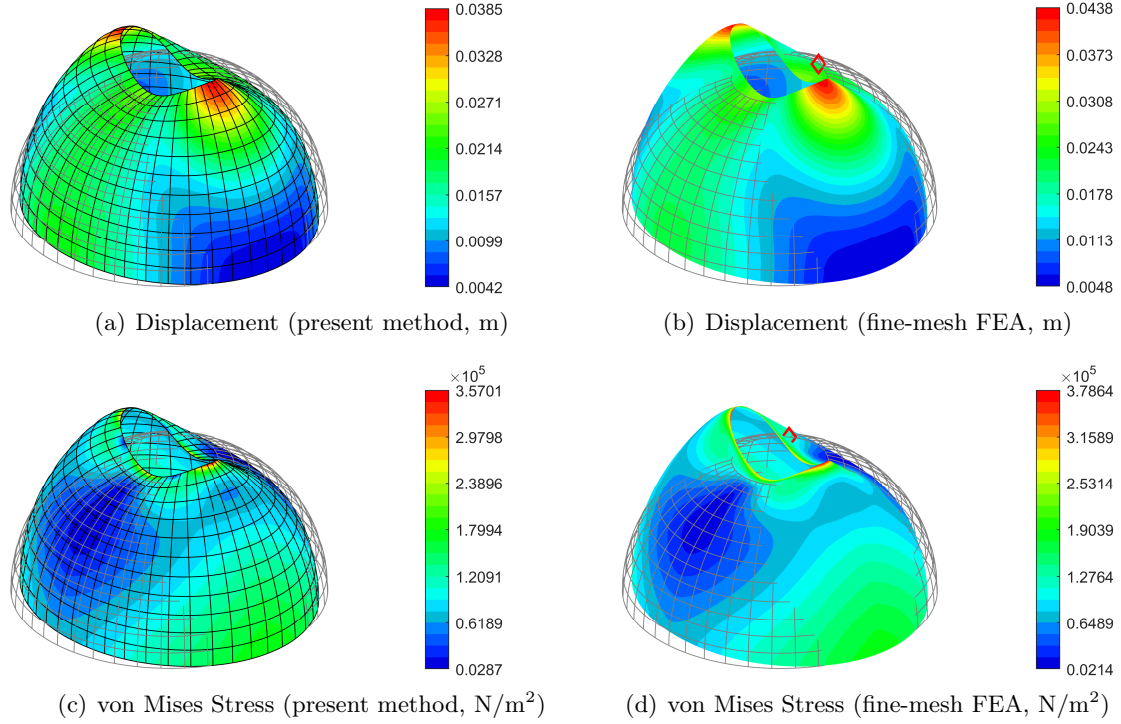


Figure 9: Contour plots of the mid-surface of half of a three-layer spherical shell subject to surface shear forces  $p_1 = 5000 \text{ N/m}^2$ ,  $p_2 = 8000 \text{ N/m}^2$ . Basic parameters are given here:  $R = 4 \text{ m}$ ,  $h = 0.2 \text{ m}$ ,  $\lambda = [0.35, 0.3, 0.35]$ ,  $E = [6.825, 4, 6.825] \times 10^7 \text{ Pa}$ ,  $\nu = [0.3, 0.3, 0.3]$ . The red diamonds mark the positions of the maximum relative errors on the undeformed structure. (a) The magnitude of displacement given by the present framework; (b) displacement field obtained from direct FEA with extremely fine mesh; (c) the von Mises stress distribution given by the present framework; (d) the von Mises stress field obtained from fine-mesh FEA.

and stress fields are 4.89% and 5.27%, respectively. This indicates that the proposed method also excels in capturing the deformation behavior of pinched cylindrical shells under shear forces.

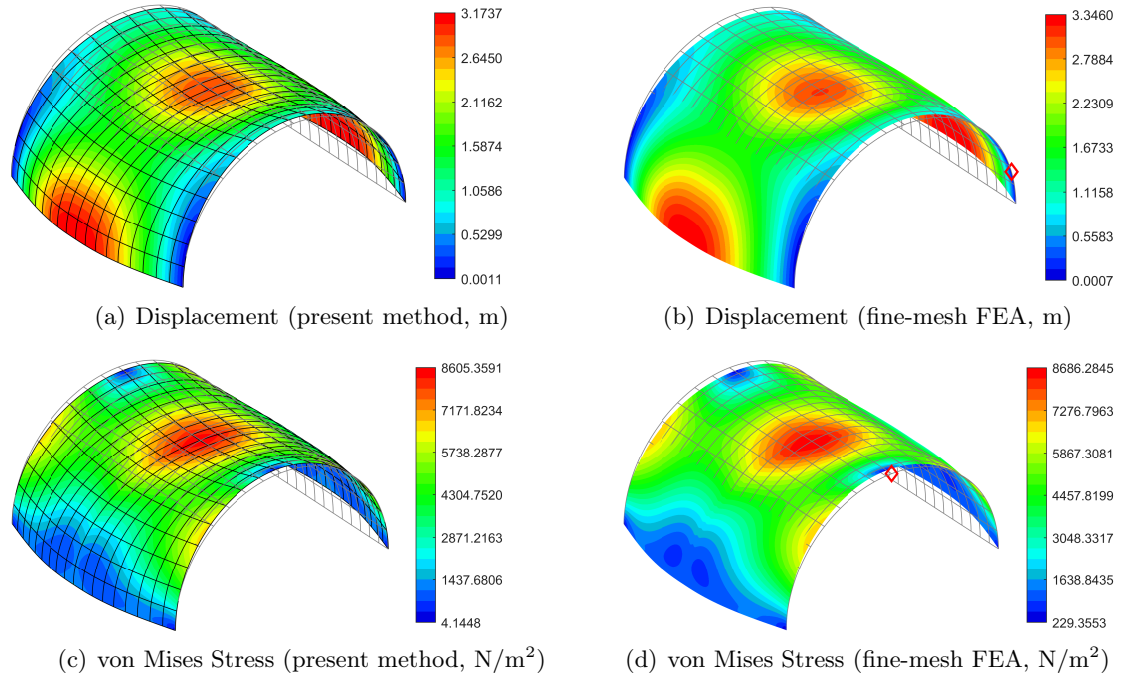


Figure 10: Contour plots of the mid-surface of a three-layer cylindrical shell subject to surface shear forces  $(p_1, p_2) = (300, 400) \text{ N/m}^2$ . Basic parameters are given here:  $R = 300 \text{ m}$ ,  $L = 600 \text{ m}$ ,  $h = 15 \text{ m}$ ,  $\lambda = [0.35, 0.3, 0.35]$ ,  $E = [3, 1.5, 3] \times 10^6 \text{ Pa}$ ,  $\nu = [0.3, 0.3, 0.3]$ . Positions of the maximum displacement and stress relative errors are shown in red diamonds. (a) The magnitude of displacement given by the present method; (b) displacement field obtained from direct FEA with extremely fine mesh; (c) the von Mises stress distribution given by the present method; (d) the von Mises stress field obtained from fine-mesh FEA.

The case of a multi-layered ellipsoidal shell is also included here to test the performance of the present

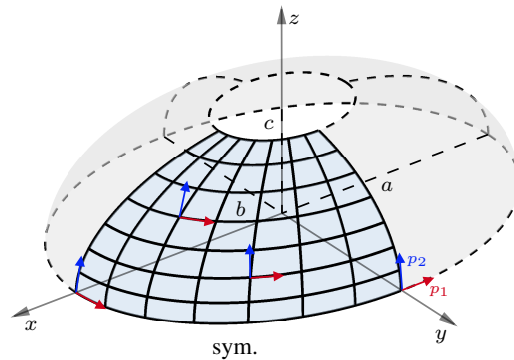


Figure 11: Illustration of the mid-surface of a three-layered ellipsoidal shell of thickness  $h = 0.2$  m, and the thickness proportion of each layer is  $\lambda = [0.35, 0.3, 0.35]$ . The lengths of three principal semi-axes are  $a = 8$  m,  $b = 6$  m,  $c = 4$  m. Note that, the NURBS parametric lines on an ellipsoid are not orthogonal, while the “lines of curvature” are not intuitive. We hence pick two such mutually orthogonal directions at each point: one aligned with  $\mathbf{r}_{\xi_1}$  and the other perpendicular to it. The components of the applied surface shear force along these two directions are  $p_1 = 5000$  N/m<sup>2</sup>,  $p_2 = 8000$  N/m<sup>2</sup>. Due to the symmetry of shell geometry and loading conditions, only one eighth of the structure (gridded part) is modeled here

model on non-classical shells. For a sphere (where all points are umbilical) and a cylinder (which has no umbilical points), the principal directions at each point can be uniformly defined, whereas the four umbilical points on an ellipsoidal surface are isolated, making it difficult to pick a local coordinate system that is coordinated with the surroundings. Therefore, as stated in Sec. 4, the local displacement field is finally transformed into the global coordinate system to circumvent the stress singularities associated with an ellipsoidal local coordinate system. The basic parameter settings regarding the ellipsoid are illustrated in Fig. 11, and the material properties assigned to each layer from bottom to top are  $E = [6.825, 4, 6.825] \times 10^7$  Pa,  $\nu = [0.3, 0.3, 0.3]$ .

The deformation modes of the mid-surface of the investigated ellipsoidal shell are shown in Fig. 12. By comparing the results given by the present method (Figs. 12(a) and 12(c)) with those given by direct finite element simulation (Figs. 12(b) and 12(d)), we can find that differences in both displacement and von Mises stress fields are mainly concentrated near the free boundary. And the largest relative errors in these two fields, marked by the red diamonds, are also located on the free edge. We can therefore attribute this to the BL effects, which are inherent in the plate and shell theories.

The averaged relative error for the displacement field is 4.79%, while that for the von Mises stress is 4.97%. It is worth mentioning that, errors of the examples discussed here are both of order  $\epsilon = 0.05$  which is exactly the theoretical accuracy of the AA method. It follows that the MTS can be modeled to a high accuracy based solely on the geometric characteristic that the shell thickness is much smaller than its corresponding surface dimensions, without requiring the introduction of the SCF or pre-assumed deformation patterns. This holds true except in the BL regions, where traditional shell theories, such as the Kirchhoff-Love theory, the FSDT, etc., also fail to provide accurate descriptions.

From the numerical examples given above, it can be seen that the leading-order equations derived from AA alone are able to capture the deformation modes of multi-layered shells under shear loading effectively without introducing additional parameters (e.g., the SCF, etc.). This suggests the actual role of the applied surface shear force, i.e., it mainly affects the redistribution of in-plane stress components (refer to Eqs. (51a) and (51b)) rather than changing the transverse shear stresses.

## 6. Conclusions And Discussions

In the present article, we propose a method within the framework of AA for modeling and interpreting the deformation behavior of multi-layered shells with greater mathematical rigor. With the help of AA, we revisit conclusions originally based on assumptions, establishing a more solid foundation. The novelties presented can be summarized into three main strands.

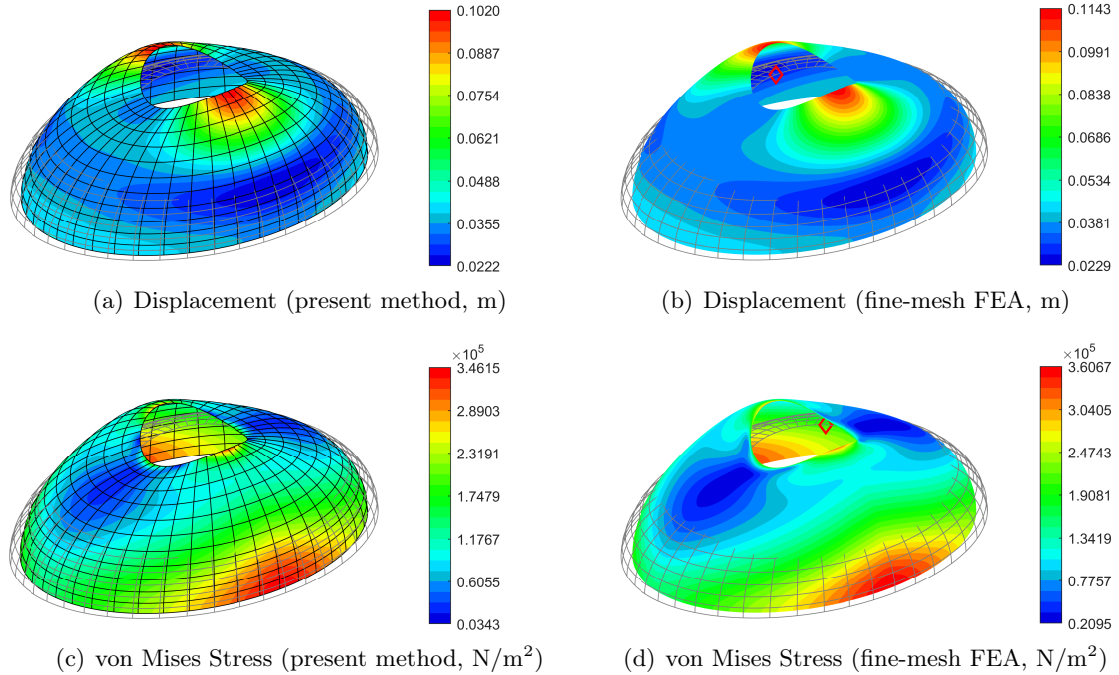


Figure 12: Contour plots of the mid-surface of a three-layer ellipsoidal shell subject to surface shear forces  $(p_1, p_2) = (5000, 8000) \text{ N/m}^2$ . The geometry of the shell mid-surface is presented in Fig. 11. Other basic parameters are given here:  $h = 0.2 \text{ m}$ ,  $\lambda = [0.35, 0.3, 0.35]$ ,  $E = [6.825, 4, 6.825] \times 10^7 \text{ Pa}$ ,  $\nu = [0.3, 0.3, 0.3]$ . Positions of the maximum displacement and stress relative errors are shown in red diamonds. (a) The magnitude of displacement predicted by the present method; (b) displacement field obtained from direct FEA with extremely fine mesh; (c) the von Mises stress distribution predicted by the present method; (d) the von Mises stress field obtained from fine-mesh FEA.

Firstly, the mechanical behavior of the elastic MTS are reconsidered based on their intrinsic thinness from the perspective of AA. The classical Kirchhoff-Love hypothesis on thin shells is well justified through the direct application of AA to the 3D governing equations and constitutive laws. This scheme also facilitates the rational formulation of both the overall stiffness and the relevant stress components. Moreover, the transverse stress components identified, although smaller compared to the in-plane stresses, are indeed nonzero.

Secondly, we classify shell deformation modes based on principal curvatures, distinguishing between cases where the maximum non-dimensional principal curvature approaches zero (resembling thin plates) and where it is of  $\mathcal{O}(1)$ , as shown in Secs. 3.3.1 and 3.3.2. In both scenarios, AA allows us to determine precise orders of relevant quantities, revealing insights into the distribution of transverse shear stresses as well as the eigenvalue problems associated with free vibrations.

Thirdly, a leading-order shell theory obtained from AA suffices to provide accurate predictions for shell stiffness and the desired stress distribution, which differs from the existing arguments requiring the inclusion of transverse shear stresses for analyzing an applied shear load on the shell surface. To be specific, the applied external shear force is shown to primarily affect the redistribution of local in-plane stress components  $\sigma_{\alpha\beta}^{(0)}$  (as implied by Eqs. (51a) and (51b)), rather than necessitating a significant consideration of transverse shear stress.

Although the current method has demonstrated certain superiority in achieving a rational understanding of the deformation behavior of shell structures, discussions of the associated model errors are still necessary. Specifically, solutions derived from the leading-order equations convergences to the real one only when the introduced aspect ratio (Eq. (20)) tends to zero, acknowledging that all shell structures inherently exist in 3D space where thickness is a small but non-negligible quantity compared to surface dimensions. Therefore, inherent errors in the leading-order model can only be minimized by reducing the aspect ratio or employing higher-order expansions, with truncation errors of the same order-of-magnitude as  $\epsilon$ .

Moreover, accurate description of deformation near the shell boundaries (especially for free and fixed boundaries) remains a challenge. The strain energy is generally concentrated along the edges of the shell mid-surface owing to curvature discontinuities, incompatible boundary conditions and/or irregular loadings, and this is known as the “BL effects”. As has been demonstrated numerically by Lee & Bathe

(2002), the strain energy, bending energy and membrane energy do not asymptotically approach zero; on the contrary, their magnitudes become increasingly singular as the thickness ratio  $\epsilon$  decreases. Fortunately, they also tend to be more concentrated near the free boundary, which means the width of the BL shrinks. Therefore, traditional shell theories that excel in the shell interior may struggle near boundaries. Addressing this requires a fully three-dimensional model regarding the BL, which consequently leads to modified boundary conditions for the investigated problem (Green (1962), Howell et al. (2008)).

Furthermore, shell analysis based on orthogonal curvilinear coordinates coinciding with “lines of curvature” of the shell mid-surface is considered to be complex and inefficient. Although such shape-dependent descriptions can effectively capture conclusions related to shell deformation patterns, they lack flexibility when faced with more complex shapes. So, in order to extend the model to arbitrary mid-surface geometries and geometric nonlinearities, adopting the invariant tensor notation (first proposed by Lurie (1940) for linear shell description) offers a more direct approach.

Finally, future studies should explore the systematic analysis of shell structures carrying microstructural details, referred to as “microstructural thin shells”, using the aforementioned invariant tensor notation within the framework of AA. Additionally, the role of shear strain in laminated structures composed of soft and hard materials can also be investigated through detailed AA.

## Acknowledgements

The financial supports from the National Natural Science Foundation of China [12172074, Zhu], and the Fundamental Research Funds for the Central Universities, P.R. China [Zhu] are gratefully acknowledged.

## Appendix A. Derivation Related to the Normal Shell

Here we will prove that the scaling relations Eqs. (38) and (39) hold for the case of normal shell in Sec. 3.3.2. First, at  $\mathcal{O}(\epsilon)$ , the constitutive relations (Eqs. (28a),(28c) and (28f)) give that

$$\begin{cases} - (1 - \nu_\mathcal{L})\widehat{u}_3^{(0)}\widehat{\kappa}_1 - \nu_\mathcal{L}\widehat{u}_3^{(0)}\widehat{\kappa}_2 + \nu_\mathcal{L}\frac{\partial\widehat{u}_3^{(1)}}{\partial\widehat{\xi}_3} = 0; \\ - \nu_\mathcal{L}\widehat{u}_3^{(0)}\widehat{\kappa}_1 - (1 - \nu_\mathcal{L})\widehat{u}_3^{(0)}\widehat{\kappa}_2 + \nu_\mathcal{L}\frac{\partial\widehat{u}_3^{(1)}}{\partial\widehat{\xi}_3} = 0; \\ - \nu_\mathcal{L}\widehat{u}_3^{(0)}\widehat{\kappa}_1 - \nu_\mathcal{L}\widehat{u}_3^{(0)}\widehat{\kappa}_2 + (1 - \nu_\mathcal{L})\frac{\partial\widehat{u}_3^{(1)}}{\partial\widehat{\xi}_3} = 0, \end{cases} \quad (\text{A.1})$$

only the trivial solution is obtained from the above equations, i.e.,

$$\widehat{u}_3^{(0)} = 0; \quad \frac{\partial\widehat{u}_3^{(1)}}{\partial\widehat{\xi}_3} = 0, \quad (\text{A.2})$$

thus the correctness of Eq. (37b) is proved. Furthermore, Eq. (A.2) implies that, under this circumstance, the three local displacement components  $u_i$  are actually of the same order-of-magnitude ( $\mathcal{O}(\epsilon)$ ), since the leading-order out-plane displacement is trivial at every point inside the shell, including umbilic points.

Next we consider the first two orders of the constitutive laws related to two transverse shear stresses Eqs. (28d) and (28e). They are

$$\begin{cases} \mathcal{O}(1) : \frac{1}{\widehat{a}_\alpha} \frac{\partial\widehat{u}_3^{(0)}}{\partial\widehat{\xi}_\alpha} + \frac{\partial\widehat{u}_\alpha^{(0)}}{\partial\widehat{\xi}_3} = 0; \end{cases} \quad (\text{A.3a})$$

$$\begin{cases} \mathcal{O}(\epsilon) : \frac{\partial\widehat{u}_\alpha^{(1)}}{\partial\widehat{\xi}_3} = -\frac{1}{\widehat{a}_\alpha} \left( \frac{\partial\widehat{u}_3^{(1)}}{\partial\widehat{\xi}_\alpha} + \widehat{\kappa}_\alpha\widehat{\xi}_3 \frac{\partial\widehat{u}_3^{(0)}}{\partial\widehat{\xi}_\alpha} \right) - \widehat{u}_\alpha^{(0)}\widehat{\kappa}_\alpha, \end{cases} \quad (\text{A.3b})$$

based on the conclusion  $\widehat{u}_3^{(0)} = 0$ , Eq. (A.3a) implies that the leading-order in-plane displacements  $\widehat{u}_\alpha^{(0)}$  satisfy

$$\frac{\partial\widehat{u}_\alpha^{(0)}}{\partial\widehat{\xi}_3} = 0, \quad \text{for } \alpha = 1, 2, \quad (\text{A.4})$$

which further leads to their sole dependence on the surface parameters, i.e., Eq. (37a). In this way, the displacement scaling relations of Eq. (38) are obtained naturally.

With the use of Eqs. (A.2) and (A.4), the left term of Eq. (A.3b) is found to be independent of the normal coordinate  $\widehat{\xi}_3$ , and another relation on the first-order in-plane displacements is then obtained by taking partial derivative w.r.t.  $\widehat{\xi}_3$ , that is

$$\frac{\partial^2 \widehat{u}_\alpha^{(1)}}{\partial \widehat{\xi}_3^2} = 0, \quad (\text{A.5})$$

we can accordingly assume that  $\widehat{u}_\alpha^{(1)}$  take the form

$$\widehat{u}_\alpha^{(1)} = f_\alpha^* \left( \widehat{\xi}_1, \widehat{\xi}_2 \right) + f_\alpha \left( \widehat{\xi}_1, \widehat{\xi}_2 \right) \widehat{\xi}_3, \quad (\text{A.6})$$

where  $f_\alpha^* \left( \widehat{\xi}_1, \widehat{\xi}_2 \right)$  and  $f_\alpha \left( \widehat{\xi}_1, \widehat{\xi}_2 \right)$  are just functions of  $\widehat{\xi}_1$  and  $\widehat{\xi}_2$ .

Now we proceed to investigate the stress components. Due to the modification of displacements scaling rules for this case, it is necessary to re-examine the order relations of stress components given above, which requires analyzing the magnitude of stresses from scratch according to the original equilibrium equations in the curvilinear coordinate system.

A detailed examination of Eq. (12) reveals that the transverse shear stresses  $\sigma_{\alpha 3}$  remain one order higher than the in-plane components  $\sigma_{\alpha\beta}$ , since there is no new difference here introduced by the premise of appreciable curvature (i.e., Eq. (36)). However, this is not true for the equilibrium equation in the thickness direction (i.e.,  $i = 3$  for Eq. (12)). To be specific, Eq. (36) allows the terms relating to in-plane normal stresses to dominate over  $\sigma_{\alpha 3}$  in this equation, so that the transverse normal stress  $\sigma_{33}$ , like the transverse shear stresses, is only one order higher than  $\sigma_{\alpha\beta}$ . The modified local stress scalings (Eq. (39)) are also proved.

We then discuss further some of the intriguing conclusions that this situation (Sec. 3.3.2) leads to. With Eq. (A.3b), the formulations of the leading-order transverse shear stresses are written by

$$\begin{aligned} \widehat{\sigma}_{\alpha 3}^{(0)} &= \frac{\widehat{E}_\mathcal{L}}{2(1+\nu_\mathcal{L})} \left[ \frac{1}{\widehat{a}_\alpha} \frac{\partial \widehat{u}_3^{(2)}}{\partial \widehat{\xi}_\alpha} + \widehat{\kappa}_\alpha \widehat{\xi}_3 \left( \frac{1}{\widehat{a}_\alpha} \frac{\partial \widehat{u}_3^{(1)}}{\partial \widehat{\xi}_\alpha} + \frac{\widehat{\kappa}_\alpha \widehat{\xi}_3}{\widehat{a}_\alpha} \frac{\partial \widehat{u}_3^{(0)}}{\partial \widehat{\xi}_\alpha} + \widehat{u}_\alpha^{(0)} \widehat{\kappa}_\alpha \right) + \widehat{u}_\alpha^{(1)} \widehat{\kappa}_\alpha + \frac{\partial \widehat{u}_\alpha^{(2)}}{\partial \widehat{\xi}_3} \right] \\ &= \frac{\widehat{E}_\mathcal{L}}{2(1+\nu_\mathcal{L})} \left( \frac{1}{\widehat{a}_\alpha} \frac{\partial \widehat{u}_3^{(2)}}{\partial \widehat{\xi}_\alpha} + \widehat{u}_\alpha^{(1)} \widehat{\kappa}_\alpha + \frac{\partial \widehat{u}_\alpha^{(2)}}{\partial \widehat{\xi}_3} - \widehat{\kappa}_\alpha \widehat{\xi}_3 \frac{\partial \widehat{u}_\alpha^{(1)}}{\partial \widehat{\xi}_3} \right). \end{aligned} \quad (\text{A.7})$$

From the  $\mathcal{O}(\epsilon^2)$  identity of the non-dimensional constitutive law regarding  $\widehat{\sigma}_{33}$  ((28f)), it can be seen that the equation  $\partial^2 \widehat{u}_3^{(2)} / \partial \widehat{\xi}_3^2 = 0$  holds, which in turn leads to the finding that the leading-order in-plane stress components  $\widehat{\sigma}_{\alpha\beta}^{(0)}$  of a point inside the TLS are equal to those at the point where it is projected along the normal to the midsurface. Thus, taking the derivative of both Eqs. (41a) and (41b) w.r.t. variable  $\widehat{\xi}_3$  yields the identity

$$\frac{\partial^2 \widehat{\sigma}_{\alpha 3}^{(0)}}{\partial \widehat{\xi}_3^2} = 0, \quad (\text{A.8})$$

then substituting Eq. (A.7) into Eq. (A.8) gives

$$\frac{\partial^2}{\partial \widehat{\xi}_3^2} \left( \frac{1}{\widehat{a}_\alpha} \frac{\partial \widehat{u}_3^{(2)}}{\partial \widehat{\xi}_\alpha} + \frac{\partial \widehat{u}_\alpha^{(2)}}{\partial \widehat{\xi}_3} \right) = 0, \quad (\text{A.9})$$

and we can similarly assume that

$$\frac{1}{\widehat{a}_\alpha} \frac{\partial \widehat{u}_3^{(2)}}{\partial \widehat{\xi}_\alpha} + \frac{\partial \widehat{u}_\alpha^{(2)}}{\partial \widehat{\xi}_3} = g_\alpha^* \left( \widehat{\xi}_1, \widehat{\xi}_2 \right) + g_\alpha \left( \widehat{\xi}_1, \widehat{\xi}_2 \right) \widehat{\xi}_3. \quad (\text{A.10})$$

Incorporating Eqs. (A.6) and (A.10) into Eq. (A.7), the simplified formulation for  $\widehat{\sigma}_{\alpha 3}^{(0)}$  is derived, that is,

$$\widehat{\sigma}_{\alpha 3}^{(0)} = \frac{\widehat{E}_\mathcal{L}}{2(1+\nu_\mathcal{L})} \left[ G_\alpha \left( \widehat{\xi}_1, \widehat{\xi}_2 \right) + g_\alpha \left( \widehat{\xi}_1, \widehat{\xi}_2 \right) \widehat{\xi}_3 \right], \quad (\text{A.11})$$

where  $G_\alpha(\widehat{\xi}_1, \widehat{\xi}_2) = \widehat{\kappa}_\alpha f_\alpha^*(\widehat{\xi}_1, \widehat{\xi}_2) + g_\alpha^*(\widehat{\xi}_1, \widehat{\xi}_2)$ . Note that, the leading-order transverse shear stress components  $\widehat{\sigma}_{\alpha 3}^{(0)}$  are actually piecewise linear w.r.t. the thickness coordinate  $\widehat{\xi}_3$ , which means that  $\widehat{\sigma}_{\alpha 3}^{(0)}$  show straight zigzag distributions and equal to the imposed shear forces on the top and bottom surfaces of the MTS if viewed from a cross-section perpendicular to the shell mid-surface, as illustrated in Fig. 7. Thus, Eq. (40) is justified. In particular, for one-layer thin shells, the leading-order transverse shear stresses can be readily determined by the surface boundary conditions given by Eq. (17).

## Appendix B. Derivation of the Jacobian Determinants Related to Domain Transformation

Now we derive the specific expressions for several Jacobian determinants in Eqs. (64) and (65). For a vector  $\mathbf{r}_e$  in the physical space, it is equivalent in representation under global and local basis vectors, i.e.,  $\mathbf{r}_e = x_i \widehat{\mathbf{e}}_i = \widehat{\xi}_i \frac{d\widehat{\xi}_i}{\|d\widehat{\xi}_i\|}$ . Therefore, a volume infinitesimal  $d\Omega$  in the Cartesian coordinates can be transformed into one in the local orthogonal curvilinear coordinate system by a certain scaling, that is,

$$d\Omega = (d\widehat{\xi}_1, d\widehat{\xi}_2, d\widehat{\xi}_3) = \det \left( \left[ \frac{\partial \mathbf{r}_e}{\partial \widehat{\xi}_1}, \frac{\partial \mathbf{r}_e}{\partial \widehat{\xi}_2}, \frac{\partial \mathbf{r}_e}{\partial \widehat{\xi}_3} \right]^T \right) d\widehat{\xi}_1 d\widehat{\xi}_2 d\widehat{\xi}_3, \quad (\text{B.1})$$

where  $(\cdot, \cdot, \cdot)$  denotes the triple product of three vectors. Compared with the second identity in Eq. (64), the Jacobian determinant measuring physical-to-local volume change is obtained

$$\left| J_{\Omega \rightarrow (\widehat{\mathcal{P}} \times \widehat{\xi}_3)} \right| = \det \left( \left[ \frac{\partial \mathbf{r}_e}{\partial \widehat{\xi}_1}, \frac{\partial \mathbf{r}_e}{\partial \widehat{\xi}_2}, \frac{\partial \mathbf{r}_e}{\partial \widehat{\xi}_3} \right]^T \right) = h_1 h_2 h_3, \quad (\text{B.2})$$

here Eq. (6) is adopted to derive the second identity of Eq. (B.2).

Similarly, an area infinitesimal  $d\mathcal{S}_t$  on the top surface of the TLS can be linked to one in the principal parametric space  $\widehat{\mathcal{P}}$  by

$$d\mathcal{S}_t|_{\widehat{\xi}_3=\frac{1}{2}} = (\mathbf{e}_3, d\widehat{\xi}_1, d\widehat{\xi}_2)|_{\widehat{\xi}_3=\frac{1}{2}} = (h_1 h_2)_{\widehat{\xi}_3=\frac{1}{2}} d\widehat{\xi}_1 d\widehat{\xi}_2, \quad (\text{B.3})$$

thus the Jacobian determinant associated with the physical-to-local area change is given by

$$\left| J_{\partial_t \Omega \rightarrow \widehat{\mathcal{P}}} \right| = (h_1 h_2)_{\widehat{\xi}_3=\frac{1}{2}}. \quad (\text{B.4})$$

Finally, we consider the change of variables in the last identities of both Eq. (64) and Eq. (65). As illustrated in Fig. 3, the area change brought by the regular map  $\mathcal{L}$  from the NURBS parametric space  $\mathcal{P}$  to the principal parametric space  $\widehat{\mathcal{P}}$  is determined by

$$d\widehat{\mathcal{P}} = (\mathbf{e}_3, d\widehat{\xi}_1, d\widehat{\xi}_2) = \det \left( \left[ \frac{\partial \widehat{\xi}_\alpha}{\partial \xi_\beta} \right] \right) d\mathcal{P}, \quad (\text{B.5})$$

where the determinant of the matrix  $\left[ \frac{\partial \widehat{\xi}_\alpha}{\partial \xi_\beta} \right]$  captures the effect of the change of variables between two parametric coordinates, that is,

$$\left| J_{\widehat{\mathcal{P}} \rightarrow \mathcal{P}} \right| = \det \left( \left[ \frac{\partial \widehat{\xi}_\alpha}{\partial \xi_\beta} \right] \right) = 1 / \det \left( \left[ \frac{\partial \xi_\beta}{\partial \widehat{\xi}_\alpha} \right] \right), \quad (\text{B.6})$$

note that the components  $\partial \xi_\beta / \partial \widehat{\xi}_\alpha$  are exactly the aforementioned combination coefficients for the generation of principal directions Eq. (61) and can be denoted as  $J_{\beta\alpha}$ .

With Eqs. (B.2), (B.4) and (B.6), the two Jacobian determinants involved in the last equations of the virtual work formulations are obtained by

$$\left| J_{\Omega \rightarrow (\mathcal{P} \times \xi_3)} \right| = h_1 h_2 h_3 / |J|; \quad (\text{B.7a})$$

$$\left| J_{\partial_t \Omega \rightarrow \mathcal{P}} \right| = (h_1 h_2)_{\widehat{\xi}_3=\frac{1}{2}} / |J|. \quad (\text{B.7b})$$

### Appendix C. Details of Discrete Form Equations

In this section, we will focus our attention mainly on rearranging Eqs. (64) and (65) into matrix form and providing a fully discretized system of linear algebraic equations. First, tensors involved are all re-expressed in Voigt notation, i.e.,

$$\mathbf{T} = \begin{bmatrix} T_{11} \\ T_{22} \\ T_{12} \end{bmatrix}; \quad \mathbf{M} = \begin{bmatrix} M_{11} \\ M_{22} \\ M_{12} \end{bmatrix}; \quad \boldsymbol{\varepsilon}^* = \begin{bmatrix} \varepsilon_{11}^* \\ \varepsilon_{22}^* \\ 2\varepsilon_{12}^* \end{bmatrix}; \quad \mathbf{k}^* = \begin{bmatrix} -k_{11}^* \\ -k_{22}^* \\ -2k_{12}^* \end{bmatrix}, \quad (\text{C.1})$$

where  $T_{\alpha\beta}$  and  $M_{\alpha\beta}$  follow the expressions given by Eq. (56) and can be further incorporated in the following matrix form

$$\begin{bmatrix} \mathbf{T} \\ \mathbf{M} \end{bmatrix} = \begin{bmatrix} \mathbf{A} & \mathbf{B} \\ \mathbf{B} & \mathbf{D} \end{bmatrix} \cdot \begin{bmatrix} \boldsymbol{\varepsilon}^* \\ \mathbf{k}^* \end{bmatrix} = \mathbf{D}^e \cdot [\partial_1] \mathbf{QRu}^e = \mathbf{D}^e \cdot \mathbf{Bu}^e. \quad (\text{C.2})$$

Specific expressions of the notations introduced above is given below.  $\mathbf{D}^e$  is an in-plane elasticity matrix consisting of the extensional, coupling and bending stiffness  $\mathbf{A}$ ,  $\mathbf{B}$  and  $\mathbf{D}$ , whose components are presented in Eq. (57). For layered isotropic elastic materials, the three stiffness matrices are simplified as

$$\mathbf{A} = \begin{bmatrix} \mathcal{A}_1 & \mathcal{A}_2 & 0 \\ & \mathcal{A}_1 & 0 \\ \text{sym.} & & \frac{\mathcal{A}_1 - \mathcal{A}_2}{2} \end{bmatrix}; \quad \mathbf{B} = \begin{bmatrix} \mathcal{B}_1 & \mathcal{B}_2 & 0 \\ & \mathcal{B}_1 & 0 \\ \text{sym.} & & \frac{\mathcal{B}_1 - \mathcal{B}_2}{2} \end{bmatrix}; \quad \mathbf{D} = \begin{bmatrix} \mathcal{D}_1 & \mathcal{D}_2 & 0 \\ & \mathcal{D}_1 & 0 \\ \text{sym.} & & \frac{\mathcal{D}_1 - \mathcal{D}_2}{2} \end{bmatrix}, \quad (\text{C.3})$$

and with Eq. (50), the newly-introduced quantities can be expressed by

$$\mathcal{A}_1 = \left\langle \frac{E_c}{1 - \nu_c^2} \right\rangle_0, \quad \mathcal{A}_2 = \left\langle \frac{E_c \nu_c}{1 - \nu_c^2} \right\rangle_0; \quad (\text{C.4a})$$

$$\mathcal{B}_1 = \left\langle \frac{E_c}{1 - \nu_c^2} \right\rangle_1, \quad \mathcal{B}_2 = \left\langle \frac{E_c \nu_c}{1 - \nu_c^2} \right\rangle_1; \quad (\text{C.4b})$$

$$\mathcal{D}_1 = \left\langle \frac{E_c}{1 - \nu_c^2} \right\rangle_2, \quad \mathcal{D}_2 = \left\langle \frac{E_c \nu_c}{1 - \nu_c^2} \right\rangle_2. \quad (\text{C.4c})$$

The matrix  $\mathbf{B} = [\partial_1] \mathbf{QR}$  connects the mid-surface strain and the global nodal displacement vector  $\tilde{\mathbf{u}}^n$  and is known as the strain-displacement matrix. With Eq. (45), the operator matrix  $[\partial_1]$  is written by

$$[\partial_1] = \begin{bmatrix} \frac{1}{a_1} \frac{\partial}{\partial \widehat{\xi}_1} & \frac{1}{a_1 a_2} \frac{\partial a_1}{\partial \widehat{\xi}_2} & -k_1 \\ \frac{1}{a_1 a_2} \frac{\partial a_2}{\partial \widehat{\xi}_1} & \frac{1}{a_2} \frac{\partial}{\partial \widehat{\xi}_2} & -k_2 \\ \frac{1}{a_2} \frac{\partial}{\partial \widehat{\xi}_2} - \frac{1}{a_1 a_2} \frac{\partial a_1}{\partial \widehat{\xi}_2} & \frac{1}{a_1} \frac{\partial}{\partial \widehat{\xi}_1} - \frac{1}{a_1 a_2} \frac{\partial a_2}{\partial \widehat{\xi}_1} & 0 \\ 0 & 0 & -\frac{h}{a_1} \frac{\partial}{\partial \widehat{\xi}_1} \left( \frac{1}{a_1} \frac{\partial}{\partial \widehat{\xi}_1} \right) - \frac{h}{a_1 a_2^2} \frac{\partial a_1}{\partial \widehat{\xi}_2} \frac{\partial}{\partial \widehat{\xi}_2} \\ 0 & 0 & -\frac{h}{a_2} \frac{\partial}{\partial \widehat{\xi}_2} \left( \frac{1}{a_2} \frac{\partial}{\partial \widehat{\xi}_2} \right) - \frac{h}{a_1^2 a_2} \frac{\partial a_2}{\partial \widehat{\xi}_1} \frac{\partial}{\partial \widehat{\xi}_1} \\ 0 & 0 & -2h \left( \frac{1}{a_1 a_2} \frac{\partial^2}{\partial \widehat{\xi}_1 \widehat{\xi}_2} - \frac{1}{\widehat{a}_1 \widehat{a}_2^2} \frac{\partial a_2}{\partial \widehat{\xi}_1} \frac{\partial}{\partial \widehat{\xi}_2} - \frac{1}{\widehat{a}_1^2 \widehat{a}_2} \frac{\partial a_1}{\partial \widehat{\xi}_2} \frac{\partial}{\partial \widehat{\xi}_1} \right) \end{bmatrix}, \quad (\text{C.5})$$

it is worth mentioning that, the partial derivatives taken w.r.t. the principal coordinates  $\widehat{\xi}_\alpha$  should be re-considered according to Eq. (62). The corresponding local-to-global displacement transformation matrix  $\mathbf{Q}$  is derived from the relationship  $u_i^* = \tilde{u}_j^* \tilde{\mathbf{e}}_j \cdot \mathbf{e}_i$ , thus the orthogonal matrix takes the form

$$\mathbf{Q} = [\mathbf{e}_1 \quad \mathbf{e}_2 \quad \mathbf{e}_3]^T, \quad (\text{C.6})$$

and as indicated by Eq. (68), the shape function matrix  $\mathbf{R}$  is specifically given by

$$\mathbf{R} = \begin{bmatrix} R_1(\xi_1, \xi_2) & 0 & 0 & \cdots & R_{n_{\text{cp}}}^e(\xi_1, \xi_2) & 0 & 0 \\ 0 & R_1(\xi_1, \xi_2) & 0 & \cdots & 0 & R_{n_{\text{cp}}}^e(\xi_1, \xi_2) & 0 \\ 0 & 0 & R_1(\xi_1, \xi_2) & \cdots & 0 & 0 & R_{n_{\text{cp}}}^e(\xi_1, \xi_2) \end{bmatrix}. \quad (\text{C.7})$$

The corresponding element nodal displacement vector reads

$$\mathbf{u}^e = \left[ \tilde{u}_1^1, \tilde{u}_2^1, \tilde{u}_3^1, \tilde{u}_1^2, \tilde{u}_2^2, \tilde{u}_3^2, \dots, \tilde{u}_1^{n_{cp}}, \tilde{u}_2^{n_{cp}}, \tilde{u}_3^{n_{cp}} \right]^T, \quad (\text{C.8})$$

with the element  $\tilde{u}_i^l$  indicating the  $i$ -th displacement component in the direction characterized by  $\tilde{\mathbf{e}}_i$  at the  $l$ -th control point.

By restoring the dimensions of Eqs. (52) and (54), we can rewrite the inertial force and moment vectors into a combined matrix form, that is,

$$\begin{bmatrix} \mathcal{T}^I \\ \mathcal{M}^I \end{bmatrix} = \begin{bmatrix} \mathbf{P}_1 & \mathbf{P}_2 \\ \mathbf{P}_2 & \mathbf{P}_3 \end{bmatrix} \cdot \begin{bmatrix} \ddot{\mathbf{u}}^* \\ \dot{\boldsymbol{\varphi}}^* \end{bmatrix} = \mathbf{P}^e \cdot [\partial_2] \mathbf{QR} \ddot{\mathbf{u}}^e = \mathbf{P}^e \cdot \mathbf{N} \ddot{\mathbf{u}}^e, \quad (\text{C.9})$$

here  $\mathbf{P}^e$  represents the element density matrix consisting of three introduced diagonal matrices  $\mathbf{P}_1$ ,  $\mathbf{P}_2$  and  $\mathbf{P}_3$ , which are specifically given by

$$\mathbf{P}_1 = \begin{bmatrix} \langle \rho_{\mathcal{L}} \rangle_0 & & \\ & \langle \rho_{\mathcal{L}} \rangle_0 & \\ & & \langle \rho_{\mathcal{L}} \rangle_0 \end{bmatrix}; \quad \mathbf{P}_2 = \begin{bmatrix} \langle \rho_{\mathcal{L}} \rangle_1 & & \\ & \langle \rho_{\mathcal{L}} \rangle_1 & \\ & & \langle \rho_{\mathcal{L}} \rangle_1 \end{bmatrix}; \quad \mathbf{P}_3 = \begin{bmatrix} \langle \rho_{\mathcal{L}} \rangle_2 & & \\ & \langle \rho_{\mathcal{L}} \rangle_2 & \\ & & \langle \rho_{\mathcal{L}} \rangle_2 \end{bmatrix}. \quad (\text{C.10})$$

Based on Eq. (67), the operator matrix  $[\partial_2]$  is presented as follows

$$[\partial_2] = \begin{bmatrix} 1 & 0 & 0 & 0 & 0 & 0 \\ 0 & 1 & 0 & 0 & 0 & 0 \\ 0 & 0 & 1 & -\frac{h}{a_1} \frac{\partial}{\partial \xi_1} & -\frac{h}{a_2} \frac{\partial}{\partial \xi_2} & 0 \end{bmatrix}^T, \quad (\text{C.11})$$

and the augmented shape function matrix  $\mathbf{N} = [\partial_2] \mathbf{QR}$  is thus obtained with the use of Eqs. (C.6), (C.7) and (C.11). It bridges the element nodal displacement vector  $\tilde{\mathbf{u}}^e$  and the displacement-rotation vector  $\left[ (\mathbf{u}^*)^T, (\boldsymbol{\varphi}^*)^T \right]^T$ , while the variation of the latter is given by Eq. (67).

Next, we derive the element body and surface force vectors  $\mathbf{f}^e$  and  $\mathbf{p}^e$  in Eq. (70c). As indicated by the definition of the orthonormal basis Eq. (4), the components of the body force  $\mathbf{f} = f_i \mathbf{e}_i$  in the orthogonal curvilinear coordinate system are just functions of  $\widehat{\xi}_\alpha$ , i.e.,  $f_i = f_i(\widehat{\xi}_1, \widehat{\xi}_2)$ . Therefore, from Eq. (65), the external work done by the body force is simplified to a surface integral defined on the shell mid-surface  $\mathcal{S}$  after homogenization along the thickness direction. In this way, the element body force vector reads

$$\mathbf{f}^e = [f_1, f_2, f_3]^T. \quad (\text{C.12})$$

Combining Eqs. (65) and (67), the element surface force vector  $\mathbf{p}^e$  takes the following form

$$\mathbf{p}^e = \left[ p_1, p_2, p_3 - \frac{h}{2} \left( \frac{p_1}{a_1} \frac{\partial}{\partial \widehat{\xi}_1} - \frac{p_2}{a_2} \frac{\partial}{\partial \widehat{\xi}_2} \right) \right]^T. \quad (\text{C.13})$$

So far, the key parameters involved have been re-expressed as matrices (or vectors). This allows us to obtain the element mass and stiffness matrix and the nodal force vector presented in Eq. (70), which are further assembled to derive the global linear algebraic equations (Eq. (69)) for the nodal displacements at control points.

## References

- Abrate, S., & Di Sciuva, M. (2017). Equivalent single layer theories for composite and sandwich structures: A review. *Composite Structures*, 179, 482–494.
- Barbero, E., Reddy, J., & Teply, J. (1990). General two-dimensional theory of laminated cylindrical shells. *AIAA journal*, 28, 544–553.
- Belytschko, T., Stolarski, H., Liu, W. K., Carpenter, N., & Ong, J. S. (1985). Stress projection for membrane and shear locking in shell finite elements. *Computer Methods in Applied Mechanics and Engineering*, 51, 221–258. URL: <https://www.sciencedirect.com/science/article/pii/0045782585900350>. doi:[https://doi.org/10.1016/0045-7825\(85\)90035-0](https://doi.org/10.1016/0045-7825(85)90035-0).



- Birman, V., & Bert, C. W. (2002). On the choice of shear correction factor in sandwich structures. *Journal of Sandwich Structures & Materials*, 4, 83–95.
- Byrne, R. (1944). *Theory of small deformations of the thin elastic shell* volume 21. University of California Press.
- Carrera, E. (2001). Developments, ideas, and evaluations based upon reissner’s mixed variational theorem in the modeling of multilayered plates and shells. *Appl. Mech. Rev.*, 54, 301–329.
- Carrera, E. (2003a). Historical review of zig-zag theories for multilayered plates and shells. *Appl. Mech. Rev.*, 56, 287–308.
- Carrera, E. (2003b). Theories and finite elements for multilayered plates and shells: a unified compact formulation with numerical assessment and benchmarking. *Archives of Computational Methods in Engineering*, 10, 215–296.
- Carrera, E., Cinefra, M., Petrolo, M., & Zappino, E. (2014). *Finite element analysis of structures through unified formulation*. John Wiley & Sons.
- Chien, W.-Z. (1944). The intrinsic theory of thin shells and plates. i. general theory. *Quarterly of Applied Mathematics*, 1, 297–327.
- Ciarlet, P. G., & Lods, V. (1996). Asymptotic analysis of linearly elastic shells. i. justification of membrane shell equations. *Archive for rational mechanics and analysis*, 136, 119–161.
- Ciarlet, P. G., & Mardare, C. (2019). Asymptotic justification of the intrinsic equations of koiter’s model of a linearly elastic shell. *Comptes Rendus Mathématique*, 357, 99–110.
- Cicala, P. (1965). *Systematic approximation approach to linear shell theory*. Libreria Editrice Universitaria Levrotto & Bella.
- COMSOL Multiphysics<sup>®</sup> v. 5.6. (2020). [cn.comsol.com](http://cn.comsol.com). COMSOL AB, Stockholm, Sweden.
- Dong, S., & Tso, F. (1972). On a laminated orthotropic shell theory including transverse shear deformation, .
- Du, X., Zhao, G., Wang, W., Guo, M., Zhang, R., & Yang, J. (2020). Nliga: A matlab framework for nonlinear isogeometric analysis. *Computer Aided Geometric Design*, 80, 101869.
- Flügge, W. (2013). *Stresses in shells*. Springer Science & Business Media.
- Gander, W., Golub, G. H., & von Matt, U. (1989). A constrained eigenvalue problem. *Linear Algebra and its Applications*, 114–115, 815–839. URL: <https://www.sciencedirect.com/science/article/pii/0024379589904941>. doi:[https://doi.org/10.1016/0024-3795\(89\)90494-1](https://doi.org/10.1016/0024-3795(89)90494-1). Special Issue Dedicated to Alan J. Hoffman.
- Green, A. E. (1962). Boundary-layer equations in the linear theory of thin elastic shells. *Proceedings of the Royal Society of London. Series A. Mathematical and Physical Sciences*, 269, 481–491.
- Gruttmann, F., & Wagner, W. (2017). Shear correction factors for layered plates and shells. *Computational Mechanics*, 59, 129–146.
- Howell, P., Kozyreff, G., & Ockendon, J. (2008). Appendix: Orthogonal curvilinear coordinates. In *Applied Solid Mechanics* Cambridge Texts in Applied Mathematics (p. 428–439). Cambridge University Press. doi:[10.1017/CB09780511611605.012](https://doi.org/10.1017/CB09780511611605.012).
- Hughes, T. J., Cottrell, J. A., & Bazilevs, Y. (2005). Isogeometric analysis: Cad, finite elements, nurbs, exact geometry and mesh refinement. *Computer methods in applied mechanics and engineering*, 194, 4135–4195.
- Kiendl, J., Bletzinger, K.-U., Linhard, J., & Wüchner, R. (2009). Isogeometric shell analysis with kirchhoff–love elements. *Computer methods in applied mechanics and engineering*, 198, 3902–3914.

- Kiendl, J., Hsu, M.-C., Wu, M. C., & Reali, A. (2015). Isogeometric kirchhoff–love shell formulations for general hyperelastic materials. *Computer Methods in Applied Mechanics and Engineering*, *291*, 280–303.
- Klinkel, S., Gruttmann, F., & Wagner, W. (1999). A continuum based three-dimensional shell element for laminated structures. *Computers & Structures*, *71*, 43–62.
- Koiter, W. (1960). A consistent first approximation in the general theory of thin elastic shells. *The theory of thin elastic shells*, (pp. 12–33).
- Lee, P.-S., & Bathe, K.-J. (2002). On the asymptotic behavior of shell structures and the evaluation in finite element solutions. *Computers & structures*, *80*, 235–255.
- Love, A. (1892). A treatise on the mathematical theory of elasticity.
- Lurie, A. (1940). General theory of elastic thin shells. *Prikl. Mat. Mech. (PMM)*, *4*, 7–34.
- Macneal, R. H., & Harder, R. L. (1985). A proposed standard set of problems to test finite element accuracy. *Finite elements in analysis and design*, *1*, 3–20.
- Mindlin, R. D. (1951). Influence of rotatory inertia and shear on flexural motions of isotropic, elastic plates. *Journal of Applied Mechanics*, *18*.
- Naghdi, P. (1957a). On the theory of thin elastic shells. *Quarterly of applied Mathematics*, *14*, 369–380.
- Naghdi, P. M. (1957b). The effect of transverse shear deformation on the bending of elastic shells of revolution. *Quarterly of Applied Mathematics*, *15*, 41–52.
- Nguyen-Thanh, N., Kiendl, J., Nguyen-Xuan, H., Wüchner, R., Bletzinger, K.-U., Bazilevs, Y., & Rabczuk, T. (2011). Rotation free isogeometric thin shell analysis using pht-splines. *Computer Methods in Applied Mechanics and Engineering*, *200*, 3410–3424.
- Piegl, L., & Tiller, W. (1997). Rational b-spline curves and surfaces. In *The NURBS Book* (pp. 117–139). Berlin, Heidelberg: Springer Berlin Heidelberg. URL: [https://doi.org/10.1007/978-3-642-59223-2\\_4](https://doi.org/10.1007/978-3-642-59223-2_4). doi:10.1007/978-3-642-59223-2\_4.
- Ram, Y. (2010). A constrained eigenvalue problem and nodal and modal control of vibrating systems. *Proceedings of the Royal Society A: Mathematical, Physical and Engineering Sciences*, *466*, 831–851.
- Reissner, E. (1941). A new derivation of the equations for the deformation of elastic shells. *American Journal of Mathematics*, *63*, 177–184.
- Reissner, E. (1945). The effect of transverse shear deformation on the bending of elastic plates, .
- Reissner, E. (1950). On a variational theorem in elasticity. *Journal of Mathematics and Physics*, *29*, 90–95.
- Reissner, E. (1952). Stress strain relations in the theory of thin elastic shells. *Journal of Mathematics and Physics*, *31*, 109–119.
- Reissner, E., & Stavsky, Y. (1961). Bending and stretching of certain types of heterogeneous aeolotropic elastic plates, .
- Sanders, J. L. (1960). *An improved first-approximation theory for thin shells* volume 24. US Government Printing Office.
- Tornabene, F., Viscoti, M., & Dimitri, R. (2022a). Equivalent single layer higher order theory based on a weak formulation for the dynamic analysis of anisotropic doubly-curved shells with arbitrary geometry and variable thickness. *Thin-Walled Structures*, *174*, 109119. URL: <https://www.sciencedirect.com/science/article/pii/S0263823122001306>. doi:<https://doi.org/10.1016/j.tws.2022.109119>.

- Tornabene, F., Viscoti, M., & Dimitri, R. (2022b). Generalized higher order layerwise theory for the dynamic study of anisotropic doubly -curved shells with a mapped geometry. *Engineering Analysis with Boundary Elements*, 134, 147–183. URL: <https://www.sciencedirect.com/science/article/pii/S0955799721002630>. doi:<https://doi.org/10.1016/j.enganabound.2021.09.017>.
- Vlasov, V. (1951). Basic differential equations in general theory of elastic shells. *Prikladnaia Matematika I Mekhanika*, 8.
- Whitney, J. (1973). Shear correction factors for orthotropic laminates under static load, .
- Zhao, X., Sun, Z., Zhu, Y., & Yang, C. (2022). Revisiting kirchhoff–love plate theories for thin laminated configurations and the role of transverse loads. *Journal of Composite Materials*, 56, 1363–1377.
- Zhao, X., & Zhu, Y. (2023). A general leading-order asymptotic theory of thin microstructural plates and uncertainty quantification of the elastic performance of composite laminates. *Journal of Composite Materials*, 57, 3145–3171.